Adaptive Linear Predictive Model of an Improved Predictive Control of Permanent Magnet Synchronous Motor Over Different Speed Regions

Moustafa Magdi Ismail, Wei Xu, *Senior Member, IEEE*, Jian Ge, Yirong Tang, *Student Member, IEEE*, Abdul Khalique Junejo, *Member, IEEE*, and Mohamed G. Hussien, *Graduate Student Member, IEEE*

***Abstract*—Model predictive control (MPC) strategy can provide significant benefits for controlling nonlinear systems over classical cascade field-oriented control (FOC). However, the MPC is still in the development stage for a high-performance predictive model. Therefore, the proposed MPC in this article updates the internal linear predictive model at each time step to accurately represent the nonlinear plant of a permanent-magnet synchronous motor (PMSM) plant over different speed regions. In other words, the adaptive discrete linear plant model (ADLPM) is designed to update the current operating conditions of the machine parameters and the equilibrium points of the measured stator currents, speed, and load torque. For the operation in the flux-weakening region, the proposed MPC depends on a performance control algorithm (PCA) to obtain high dynamic performance. In this PCA algorithm, the proposed MPC depends on the modified reference velocity rather than the original reference velocity, which can calculate the required *d*-axis current directly. Moreover, the proposed cost function is designed directly in terms of the error values of the velocity and *d*-axis current, which fits the motor performance based on the further constraint of the maximum magnitude of the drawn stator current provided to control the acceleration of the rotor. Finally, comprehensive simulations and experiments have fully demonstrated that the proposed MPC can reduce the speed drop, and torque ripple in response to those of the FOC and traditional MPC strategies.**

Manuscript received 28 March 2022; revised 20 June 2022; accepted 23 July 2022. Date of publication 29 July 2022; date of current version 6 September 2022. This work was supported in part by the National Natural Science Foundation of China under Grant 51877093, in part by the Shenzhen International Collaboration under Grant GJHZ20210705142539007, in part by the Key Research and Development Program of Sichuan Province under Grant 2021YFG0081, and in part by the Technology and Innovation Commission of Shenzhen Municipality under Grant JCYJ20190809101205546. Recommended for publication by Associate Editor R. Kennel. *(Corresponding author: Jian Ge.)*

Moustafa Magdi Ismail is with the Electrical Engineering Department, Faculty of Engineering, Minia University, Minya 61517, Egypt (e-mail: mostafa.ismaiel@mu.edu.eg).

Wei Xu, Jian Ge, and Yirong Tang are with the State Key Laboratory of Advanced Electromagnetic Engineering and Technology, School of Electrical and Electronic Engineering, Huazhong University of Science and Technology, Wuhan 430074, China (e-mail: weixu@hust.edu.cn; gejian1994@hust.edu.cn; yirtang@foxmail.com).

Abdul Khalique Junejo is with the Electrical Engineering Department, Qaid-e-Awam University of Engineering, Science and Technology, Nawabshah 67450, Pakistan (e-mail: ak.junejo@gmail.com).

Mohamed G. Hussien is with the Department of Electrical Power and Machines Engineering, Faculty of Engineering, Tanta University, Tanta 31527, Egypt (e-mail: mohamed.hussien3@f-eng.tanta.edu.eg).

Color versions of one or more figures in this article are available at https://doi.org/10.1109/TPEL.2022.3194839.

Digital Object Identifier 10.1109/TPEL.2022.3194839

***Index Terms*—Adaptive discrete linear plant model (ADLPM), flux-weakening operation, model predictive control (MPC), performance control algorithm (PCA), permanent-magnet synchronous motor (PMSM).**

I. Introduction

MODEL predictive control (MPC) has been gradually becoming one of the modern strategies in motor drives due to the increased computation power of microprocessors [1], [2]. One of the main features that make MPC a successful strategy is the independence of complex mathematical reasoning, which is intuitive and simple. Meanwhile, the fertility of MPC can be designed according to the details of the control problem, which can suit all industrial applications in theory [3]–[5]. Besides, MPC is better than sliding mode control in terms of controlled actuator performance in heavy nonlinear systems [6]. Because the MPC algorithm can consider difficult nonlinear constraints every step time, the manipulated variables are identified in terms of the proposed cost function [7]. As a result, the MPC has been employed in the control of the permanent-magnet synchronous motor (PMSM), where torque control is difficult due to unequal stator inductance [8], [9]. However, PMSM drives have become important for vehicle applications in light of their power density and high torque-to-weight ratio. Thus, it is necessary to increase the ability to regulate currents and speed in the flux-weakening region [10], [11].

The traditional concept of flux-weakening control is to control the *d*-axis current required to adapt the air-gap field over various speeds. Meanwhile, conventional strategies usually rely on cascaded proportional-integral (PI) regulators, which are difficult to tune in a highly nonlinear plant model [12], [13]. Thus, different MPC algorithms have been proposed to improve the dynamic performance of the PMSM drive systems [14]–[18]. The MPC in [14] has been proposed to control the induced torque of controlled PMSM in the flux-weakening region. Besides, it is designed based on the *d-q* axes nonlinear model and the combination of the real-time gradient method and Lagrangian method to consider heavy nonlinear constraints of the current and voltage. As a result, the proposed MPC algorithm can achieve the reference torque corresponding to the minimum current and power. However, this proposed method complains of the burden of computational operations. Besides, a direct torque MPC algorithm based on the evaluation strategy of a finite

control set is proposed in [15] for high horsepower systems. In this article, the cost function is designed to maximize the torque per ampere considering the operation in the flux-weakening region. Despite the lack of a torque observer, it can achieve high performance during operations in this region without resorting to the frequency modulation algorithm or weakening the quality of induced torque. In [16], Arpacik and Ankarali proposed an optimization procedure in a real-time mode employed in the linear MPC approach to reduce the consumed time for the computational of the optimal manipulated reference voltages. The real-time optimization algorithm is based on dual active set optimizers combined with conventional matrix update strategies. Meanwhile, the proposed real-time optimizer has been implemented to drive surface-mounted PMSM at the flux-weakening region. As a result, stable control of the stator current and torque has been achieved based on this MPC optimizer.

The improved linear MPC strategy in [17] is employed on interior magnet PMSM to reduce the copper and iron loss while it is operating in the flux-weakening region. The challenge of the MPC algorithm is to handle heavy nonlinearity constraints of stator current, voltages, and cost function. As a result, it can achieve lower copper and iron loss compared to the classical MPC algorithm in the extended speed range. The cost function is optimized in [18] in a flux increment form whose stator flux magnitude is the manipulated variable of the optimizer of the proposed linear MPC. Besides, the proposed cost function can determine the saturation degree of the voltage source inverter. Meanwhile, the outer flux control loop of the PI regulator compensates for the required flux of the *d*-axis as well as the speed outer control loop determines the reference flux of the *q*-axis. Thus, the proposed cost function has achieved high dynamic performance in the flux-weakening region without further constraints. Moreover, the linear MPC strategy in [19] has been employed to drive the open winding PMSM based on two stator flux vectors in the stator flux incremental algorithm. Meanwhile, the proposed cost function has the stator flux as a manipulated variable as well. Besides, an outer control loop is employed for compensating the required field that the PMSM will need in the flux-weakening region. Thus, it can be seen from the results that the proposed MPC can minimize the switching frequency of the dual voltage source inverters with no need for the assistant algorithm. Meanwhile, the difference in the dc-link values for the two inverters can be eliminated during work in the linear modulation region, which can select the generalized vector of the modulation technique.

The improved deadbeat MPC for stator current control in [20] has been proposed to cancel the PI regulators of the traditional inner current controllers. As a result, this proposed strategy reduces the parameter tuning burden for classical cascading PI controllers. Besides, the PI parameters of the outer speed controller can be set adaptively based on the principle of direct speed control. Thus, the proposed linear MPC has been employed on the surface PMSM to achieve stable control of the stator current and speed in operating the flux-weakening region independently with varying machine parameters. The optimal speed controller in [21] has been implemented into a linear MPC framework in terms of the inherent optimizer to drive PMSM. Meanwhile, the voltage vector actuation range and pulsewidth modulation technique in the proposed system dependent on the inner predictive torque algorithm. Thus, the proposed drive system has achieved a high dynamic performance and efficient steady-state results with an expected ripple of induced torque and stator current based on the inherent pulsewidth modulation algorithm. Besides, the finite set evaluation algorithm has been developed in [22] to improve the selection of the optimal voltage vector. The improvement is related to the boundary settings of the stator current constraint, which is calculated based on the maximum torque per ampere algorithm. Besides, the current vector can be calculated automatically to provide the boundary of the reference stator current. Thus, the proposed dynamic performance can track the reference torque and stator current more efficiently compared to the discussed classical strategy. However, the discussed results have shown to what extent the proposed strategy depends on the machine parameters. Moreover, the linear MPC algorithm in [23] has been developed based on a multistage series strategy for optimizing reference voltages. Whereas the proposed cost function aims to control the stator current through the finite set evaluation technique, it will be repeated at each stage to get the best prediction. Thus, the proposed linear current predictive control can reduce the switching frequency relative to the classical MPC strategy at the constant control frequency when it has been employed on the PMSM drive. Finally, the proposed linear MPC strategy in [24] can predict the future behavior of the interior PMSM based on two cost functions. Thus, the induced torque is maximized per ampere in terms of confirming the voltages and the stator current limits. Thus, the discussion of the results has confirmed that the induced torque of the PMSM is maximized per ampere unit in the operation of the flux-weakening region.

The nonlinear PMSM system may introduce the motivation for this article. When the PMSM is used in the traction application [7], [10], it becomes a highly nonlinear plant model. As a result, the MPC algorithm should consider controlling the dynamic state variables of the traction applications as the lateral velocity and yaw position, besides the state variables of the inherent motor model as the stator current, induced torque, and rotational velocity. Meanwhile, the MPC outcomes for each sample time are delayed because of the long prediction horizon and multiple local optimal points for the cost function. Besides, the MPC is at risk of failing to predict motor performance due to the parameter variation of the drive system, where parameters may change due to operating conditions or mismatches in machine parameters. Therefore, these reasons motivate this article to address the adaptive linear MPC strategy employed on the interior PMSM drive.

The main contributions in this article can be summarized as follows. First, the adaptive MPC updates the controller prediction model at each time step around the current operating conditions. This procedure is a computational operation to provide a time-invariant small linear signal model of the PMSM plant based on the Taylor series expansion. Generally, the internal linear model can be updated online around the new current equilibrium points of the measured stator currents of the *d-q* axes, speed, estimated electromagnetic torque, and machine parameters. As a result, the predictive model of the nonlinear

PMSM plant can be depicted in several speed regions as a discrete linear equation that can be implemented on the digital control unit. Second, the objective function components consist of the velocity error and the stator current error of the *d*-axis. Thus, the proposed adaptive MPC strategy can get much better stable control for a stator current and velocity. Besides, the flux observer of the third-order generalized integrator can calculate the induced torque as it is necessary to predict the motor speed. Hence, the motor stator inductance of the *d-q* axes can be estimated in terms of the estimated motor flux to adapt the prediction model. Finally, one performance control algorithm (PCA) is proposed to improve the dynamic performance of the PMSM. The acceleration of the PMSM rotor is controlled based on this algorithm to achieve a stable speed and reduce electric current ripple. Thus, this algorithm is linked to the proposed cost function at each step time based on the modified reference velocity, the calculation of the required *d*-axis current, and the additional constraint of the maximum magnitude of the predictive stator current.

The significance of the proposed MPC algorithm in this article is summarized as follows. First, the new adaptive discrete linear plant model (ADLPM) is generally introduced to fasten any real-time optimization algorithm because it contains exactly discrete linear terms and a few numbers of the state variables. Second, the proposed PCA is generally introduced for any motor drive and MPC strategy because this algorithm has coefficients that depend only on the maximum speed of the constant torque region. In contrast, the MPC in [25] depends on the approximate rate of maximum voltage change to determine the final *d-q* axes voltages. Finally, the proposed MPC can reduce the current ripple and transient settling time. Besides, it can reduce the speed drop during the torque disturbance period.

This article is organized as follows. First, two predictive model approaches for the MPC strategy of the PMSM drive are compared in Section II. Meanwhile, this section illustrates the MPC algorithm [25] used in performance comparison relative to the proposed adaptive MPC strategy. Second, the overall design of the proposed MPC is presented in Section III, which includes a PCA, discrete improved linear plant model, machine parameters estimation, and proposed cost function. Third, comprehensive simulation and experimental results are discussed in Sections IV and V, respectively. Finally, conclusions are drawn in Section VI.

II. Predictive Model Approaches

Often, the interior PMSM plant model of the MPC strategy is approximated precisely in a linear approach model only around a local equilibrium point. However, the issue here is that this approximated model will not be accurate with time and changing PMSM plant operating conditions. Thus, several MPC approaches are introduced in this section to solve the problem of a predictive model.

A single linear model of the PMSM plant is usually causing a loss of information, which is critical for the flux weakening operation. Precisely, the relation between the stator current and velocity or the coupled parts of the stator voltages is not considered [26]. As a result, the MPC strategy works with the nonlinear plant using a gain-scheduled MPC algorithm or a nonlinear MPC algorithm [25].

The MPC controller as proposed in [26] divides the speed range into speed regions to consider the rotor speed as a constant for every region. Thus, the coupling parts of the stator voltage can be approximated as a function of the stator current only. As a result, multiple linear predictive models are implemented in the proposed MPC. Meanwhile, the gain scheduled MPC algorithm is employed to select the desired speed region based on the measured speed. The accuracy of this MPC as proposed in [26] depends on how close the selected constant speed is to the measured speed. Thus, the output *d-q* axes stator voltages (u_{ds}, u_{qs}) of the prediction horizon are corrected to obtain a higher performance of the PMSM. Thus, the voltage is defined as

$$\begin{cases} u_{ds}(k) = u_{sd}^{\text{cmp}}(k) + u_{ds}^{\text{ctrl}}(k) \\ u_{qs}(k) = u_{qs}^{\text{cmp}}(k) + u_{qs}^{\text{ctrl}}(k) \\ u_{ds}^{\text{cmp}}(k) = -Ln_p(\omega_m(k) - \Omega_{mi})i_{qs}(k) \\ u_{qs}^{\text{cmp}}(k) = Ln_p(\omega_m(k) - \Omega_{mi})i_{ds}(k) \end{cases} \tag{1}$$

where *L* is stator inductance for the surface-mounted PMSM, n_p is the number of the pole pairs, *k* is the time step of the prediction horizon, $u^{\text{cmp}}{}_{ds}$ and $u^{\text{cmp}}{}_{qs}$ are *d-q* axes compensation voltages, and i_{ds} and i_{qs} are the *d-q* axes stator currents. This MPC method is one idea of the gain-scheduled strategy. Furthermore, the optimization technique and constraints can be tailored to each speed region. As a result, it facilitates computation and increases the memory used in the digital control unit.

The MPC in [25] is explained in terms of three different main points: consideration of electromagnetic torque, predictive plant model, and constraints. First, the load torque must be known in advance to set as a constant. However, this is a shortcoming because it is difficult to determine the required flux-weakening stator current and causes an overrun in the transient time. Second, the forward Euler is used for the predictive model to discrete the differential equations. Therefore, the predictive model can be described as

$$\begin{cases} X_c(k+1) = A_c X_c(k) + B_c U_c(k) \\ Y_c(k) = C_c X_c(k) \end{cases} \tag{2}$$

$$\begin{cases} X_c(k) = [i_{ds}(k), i_{qs}(k), \omega_m(k), i_{ds}i_{qs}(k) \\ \quad , \omega_m i_{ds}(k), \omega_m i_{qs}(k), 1]^T \\ U_c(k) = [v_{ds}(k), v_{qs}(k)]^T \\ Y_c(k) = [i_{ds}(k), i_{qs}(k), \omega_m(k)]^T \end{cases} \tag{3}$$

where $X_c(k)$ is the state vector, $U_c(k)$ is the input vector, and $Y_c(k)$ is the output vector. Moreover, the discretization matrices of the state-space representation can be given out as

$$B_c(7,2) = \begin{bmatrix} T_s/L_d & 0 \\ 0 & T_s/L_q \end{bmatrix} \text{zeros[2,5]}^{\text{T}}$$

$$C_c(7,7) = \begin{bmatrix} \text{diag}([111]) \ \text{zeros}[3,4] \\ \text{zeros}[4,7] \end{bmatrix}$$

$$A_c(7,7) = \begin{bmatrix} a_{11} & 0 & 0 & 0 & 0 & a_{16} & 0 \\ 0 & a_{22} & a_{23} & 0 & a_{25} & 0 & 0 \\ 0 & a_{32} & a_{33} & a_{34} & 0 & 0 & a_{37} \\ & \text{zeros}[4,3] & & \text{diag}([1\ 1\ 1\ 1]) & & & \end{bmatrix} \tag{4}$$

$$\begin{cases} a_{11} = 1 - (T_s R_s / L_d), a_{16} = T_s n_p L_q / L_d, a_{22} \\ \quad = 1 - (T_s R_s / L_q) \\ a_{23} = -T_s n_p \lambda_m / L_q, a_{25} = -T_s n_p L_d / L_q, a_{32} \\ \quad = 1.5 T_s n_p \lambda_m / J \\ a_{33} = B_v T_s / J + 1, a_{34} = 1.5 T_s n_p (L_d - L_q)/J, a_{37} \\ \quad = -T_s T_L / J \end{cases} \tag{5}$$

where A_c is the state matrix, B_c is the input matrix, C_c is the output matrix, J is the inertia of the shaft, T_s is the discrete controller sample time, B_v is the coefficient of viscous frictions, λ_m is the flux of the rotating magnet linking the stator, R_s is the resistance of the stator, T_L the load torque, and L_d and L_q are the stator inductances of the *d-q* axes. It can be seen from (2) to (5), that the state vector contains seven state variables. Besides, the nonlinearity terms of $\omega_m i_{ds}$ and $\omega_m i_{ds}$ would make it difficult for the optimization procedure to find the optimal control variables due to the nonconvex optimization model, or multiple local optimum points in the cost function.

Third, Liu et al. [25] proposed a constraint to get the stable speed and current that controls the change rate for the reference stator voltages as given by

$$|\Delta v_{ds}| \le \Delta v_{ds-\max}, |\Delta v_{qs}| \le \Delta v_{qs-\max} \tag{6}$$

where Δv_{ds} and Δv_{qs} and $\Delta v_{ds\text{-max}}$ and $\Delta v_{qs\text{-max}}$ are the change rates of the *d-q* axes stator voltage components and the maximum change rates, respectively. Besides, Liu et al. [25] mentioned that it was complicated to decide $\Delta v_{ds\text{-max}}$ in theory. Meanwhile, $\Delta v_{ds\text{-max}}$ and $\Delta v_{qs\text{-max}}$ can be roughly defined as

$$\Delta v_{ds-\max} = \Delta v_{qs-\max} = \frac{T_s V_{\text{dc}}}{t_s} \tag{7}$$

where t_s is required settling time. Finally, the proposed MPC strategy in this article can overcome the mentioned disadvantages of the gain scheduled and nonlinear MPC approaches by providing an adaptive linear predictive model to update the current operating conditions and machine parameters at each time step. As a result, the MPC optimizer can easily select the optimal value of the control variable. Meanwhile, the adaptive linear predictive model can accurately represent the nonlinear PMSM plant while avoiding long memory uses. Therefore, the next section will explain the proposed adaptive linear MPC strategy.

III. Analysis and Design of the Proposed MPC

The proposed PMSM drive system is shown in Fig. 1 where the following discussions refer to the shown symbols. As can be seen from this figure, the proposed MPC is implemented to drive a 3-kW PMSM. In each sample time, the embedded digital controller unit of TMS320F28335 considers the mechanical angle (θ_m) to calculate the rotor angular speed (ω_m). Meanwhile, it measures the *d-q* axes stator currents (i_{ds}, i_{qs}) and dc-link

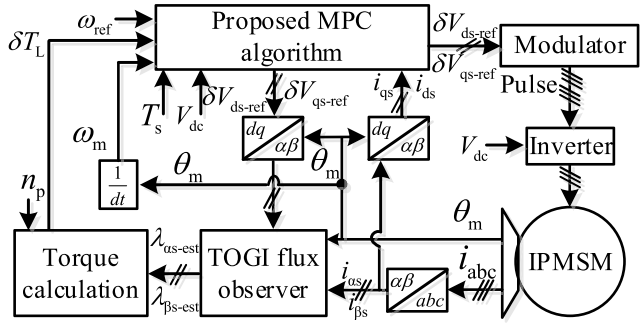

Fig. 1. Block diagram of the proposed MPC algorithm.

voltage (V_{dc}) for the input of the proposed MPC. Thus, the proposed drive is summarized as follows.

1) A flux-observer based on the TOGI is used to estimate the electromagnetic torque.
2) The proposed ADLPM is updated around the motor operating points of the sampled i_{ds}, i_{qs}, and ω_m.
3) The proposed PCA is employed to improve motor performance by computing the modified reference velocity, *d*-axis reference stator current, and maximum allowable magnitude of stator current.
4) The interior-point-convex algorithm is employed to evaluate the proposed cost function and optimize the manipulated variables of the *d-q* axes stator voltages [27]–[29]. As a result, the space vector modulation is set by the *d-q* axes stator voltages to provide the inverter pulses.

A. Adaptive Discrete Linear Predictive Model

In general, differential equations of the interior type of the PMSM can be given by

$$\begin{cases} \frac{di_{ds}}{dt} = \left(v_{ds} - R_s i_{ds} + L_q n_p \omega_m i_{qs}\right)/L_d \\ \frac{di_{qs}}{dt} = \left(v_{qs} - L_d n_p \omega_m i_{ds} - R_s i_{qs} - \lambda_m n_p \omega_m\right)/L_q \\ \frac{d\omega_m}{dt} = \left(1.5 n_p \lambda_m i_{qs} + 1.5 n_p (L_d - L_q) i_{ds} i_{qs} \right. \\ \qquad \left. - T_L - B_v \omega_m\right)/J \end{cases} \tag{8}$$

where *d/dt* refers to the first-order differential, and v_{ds} and v_{qs} are the stator voltages of the *d-q* axes, respectively.

Typically, a Taylor series expansion is used to provide a small linear signal of (8) based on the state-space representation. Thus, the proposed time-variant linear plant model can be implemented by the state-space, as illustrated by

$$\begin{cases} dx(t)/dt = A(t)x(t) + Bu(t) + E\delta T_L(t) \\ y(t) = Cx(t) + Du(t) \\ x(t) = [\delta i_{ds}(t), \delta i_{qs}(t), \delta\omega_m(t)]^T \\ u(t) = [\delta v_{ds}(t), \delta v_{qs}(t)]^T \\ y(t) = x(t) \end{cases} \tag{9}$$

where the symbol of "δ" indicates a small signal of the state variable, $x(t)$ is the state vector, $u(t)$ is the input vector, and $y(t)$ is the output vector. Meanwhile, these matrices will be linearized

and expressed as

$$A(3,3)=\begin{bmatrix} -R_s/L_d & L_q n_p\omega_{m0}/L_d & L_q n_p i_{qs0}/L_d \\ -L_d n_p\omega_{m0}/L_q & -R_s/L_q & n_p((-L_d i_{ds0})-\lambda_m)/L_q \\ 1.5n_p i_{qs0}(L_d-L_q)/J & 1.5n_p(\lambda_m+i_{ds0}(L_d-L_q))/J & -B_v/J \end{bmatrix} \tag{10}$$

$$B(3,2)=\begin{bmatrix} 1/L_d\ 0\ 0 \\ 0\ 1/L_q\ 0 \end{bmatrix}^{\mathrm{T}} \tag{11}$$

$$C(3,3)=\mathrm{diag}([111]),\ E(3,1)=\begin{bmatrix} 0\ 0\ -1/J \end{bmatrix}^{\mathrm{T}}. \tag{12}$$

As seen from (9)–(12), *A* is the state matrix, *B* is the input matrix, *C* is the output matrix, *E* is the induced torque matrix, and *D* is the feedthrough matrix is zero. As a result, i_{ds0}, i_{qs0}, and ω_{m0} are the equilibrium points to be the operating conditions of the *d-q* axes stator currents and mechanical rotor speed.

The operating points of (9) are updated in terms of the measured i_{ds}, i_{qs}, and ω_m to provide an accurate representation of the nonlinear PMSM plant. Hence, the proposed plant model can define the flux trajectory of PMSM in all speed regions. For digital implementation, the time-variant model should be transformed into a discrete model of variables that do not vary over the sample time. As a result, the operating points are updated in the state matrices for each sample time, and thus, (8) is discretized with a time step using a zero-order hold method [1] by

$$\begin{cases} x[k+1]=A_{\mathrm{d}}[k]\,x[k]+B_{\mathrm{d}}u[k]+E_{\mathrm{d}}\delta T_{\mathrm{L}}[k] \\ y[k]=Cx[k] \end{cases} \tag{13}$$

where A_d, B_d, and E_d are the discretization matrices of *A*, *B*, and *E*, respectively, and they can be calculated as

$$\begin{cases} A_d = e^{AT_{\mathrm{s}}} \\ B_d = A^{-1}(A_d-\mathrm{diag}([1\ 1\ 1]))B \\ E_d = A^{-1}(A_d-\mathrm{diag}([1\ 1\ 1]))E \end{cases}. \tag{14}$$

It is noted that the challenge in (14) is to compute e^{AT_s} accurately because the dimension of the state matrix is 3 by 3. After taking the Laplace of (14), it will get

$$A_{\mathrm{d}}(i,j)(S)=\frac{1}{\mathrm{diag}([S\ S\ S])-A(i,j)},i=1:3,j=1:3 \tag{15}$$

where *S* is the Laplace domain. Meanwhile, the order degree of the leading terms of the main diagonal elements in the matrix $A_{\mathrm{d}}(S)$ is two for the numerator and three for the denominator. However, the other elements contain a first order of the numerator and third order of the denominator. As a result, the main diagonal elements of A_d can be defined after computing the inverse Laplace using the fraction decomposition and then replacing each *t* of the time domain with T_s as

$$A_d(i,i)=q_1e^{-q_2T_{\mathrm{s}}}+q_3e^{-q_4T_{\mathrm{s}}}\cos(\theta T_s)+q_5e^{-q_6T_s}sin(\theta T_s),\ \text{at}\ i=1:3. \tag{16}$$

Besides, other elements of an A_d matrix can be defined as

$$A_d(i,j)=q_7e^{-q_8T_s}+q_9e^{-q_{10}T_s}+q_{11}e^{-q_{12}T_{\mathrm{s}}},\ i=1:3,j=1:3,\text{at}\ i\neq j \tag{17}$$

where θ and q_1 to q_{12} are variables that are closely determined by the motor parameters and the operating points.

B. Stator Inductance and Electromagnetic Torque Estimation Based on a TOGI Observer

The estimation values of the stator winding inductances and the induced torque will be clarified in this section to adapt the proposed linear predictive model across all velocity regions.

The first-order integrator suffers from dc offset and ac harmonics caused by a mismatch of machine parameters and converter nonlinearities. Therefore, the TOGI flux observer is proposed to reduce the dc and high-order components in the flux linkage. These reductions have been demonstrated in [30] compared to second-order and first-order generalized integration observers. For demonstration, the back-EMF of the controlled PMSM is analyzed by Fourier series expansion. Thus, the TOGI observer was designed based on the frequency analysis of the bode diagrams to minimize the dc and unwanted components. As a result, the discrete transfer function of the estimated α-β axes fluxes can be written as

$$\frac{\lambda_{\alpha s-\mathrm{est}}}{\delta V^*_{\alpha s-\mathrm{ref}}}=\frac{2W_0\left(1-z^{-1}-z^{-2}+z^{-3}\right)}{1+W_1z^{-1}+W_2z^{-2}+W_3z^{-3}} \tag{18}$$

$$\frac{\lambda_{\beta s-\mathrm{est}}}{\delta V^*_{\beta s-\mathrm{ref}}}=\frac{\omega_{\mathrm{c}}T_{\mathrm{s}}W_0\left(1-z^{-1}-z^{-2}+z^{-3}\right)}{1+W_1z^{-1}+W_2z^{-2}+W_3z^{-3}} \tag{19}$$

where ω_c is the center frequency, $\lambda_{\alpha s\text{-est}}$ and $\lambda_{\beta s\text{-est}}$ are the estimated fluxes in the α-β axes stationary frame, $\delta V_{\alpha s\text{-ref}}$ and $\delta V_{\beta s\text{-ref}}$ is the α-β axes of stator reference voltages, and W_0, W_1, W_2, and W_3 the integrator coefficients, respectively. More details on transfer functions and how to define them can be found in [30]. Therefore, the TOGI online flux observer is utilized as a flux estimator to calculate the electromagnetic torque (δT_{L}) and stator winding inductances of the *d-q* axes ($L_{d\text{-est}}$ and $L_{q\text{-est}}$). For calculating the electromagnetic torque (δT_{L}), the torque can be calculated from the estimated flux linkages as illustrated by

$$\delta T_L=1.5n_p(\lambda_{\alpha s-\mathrm{est}}\delta i_{\beta s}-\lambda_{\beta s-\mathrm{est}}\delta i_{\alpha s}) \tag{20}$$

where $\delta i_{\alpha s}$ and $\delta i_{\beta s}$ are α-β axes of stator currents. Besides, the online estimation of stator inductances without magnetic saturation can be considered by changing to a linear model and the flux is linearly proportional to the current in the stator windings [31], [32]. As a result, the stator inductances ($L_{d\text{-est}}$ and $L_{q\text{-est}}$) can be calculated by

$$\begin{cases} L_{d-\mathrm{est}}=(\lambda_{ds-\mathrm{est}}-\lambda_m)/i_{ds} \\ L_{d-\mathrm{est}}=\lambda_{qs-\mathrm{est}}/i_{qs} \end{cases} \tag{21}$$

where $\lambda_{ds\text{-est}}$ and $\lambda_{qs\text{-est}}$ are *d-q* axes of the estimated fluxes that can be obtained from α-β axes stationary frame using Park and inverse Clarke transformations [32]. Meanwhile, the values of ($L_{d\text{-est}}$ and $L_{q\text{-est}}$) are received from average filters to reduce the noise [31]. Finally, the proposed MPC strategy can adapt the

proposed ADLPM with values of stator inductance and torque across the prediction horizon.

C. Proposed Performance Control Algorithm (PCA)

The merits of the highly efficient PMSM drive system include stable speed, little overrun, and little current ripple. Therefore, this section proposes an algorithm for regulating the acceleration of the motor shaft during the disturbance period. Focusing on the problem, the variation in the reference velocity of the drive system is considered a disturbance of the PMSM plant. Besides, the variation in torque required for the mechanical load is also plant disturbance. Thus, the acceleration of the motor shaft is not equal to zero, and this causes an overshoot or down shoot of the motor speed and current. Therefore, the proposed MPC approach should control the shaft acceleration.

The law of rotation with neglecting the friction and the damping torque can be defined as

$$J\frac{d\omega_m}{dt} = T_m - T_e \tag{22}$$

where $d\omega_{\rm m}/dt$ is the rotor shaft acceleration, $T_{\rm e}$ is the electromagnetic torque, and T_m is the driving mechanical torque. Multiplying (22) by ω_m results in the following:

$$M\frac{d\omega_m}{dt} = P_m - P_e \tag{23}$$

$$\begin{cases} M = \frac{2W_k}{\omega_m} \\ W_k = \frac{1}{2}J\omega_m^2 \\ P_m = \omega_m T_m \\ P_e = \omega_m T_e \end{cases} \tag{24}$$

where M is the inertia constant, W_k is the kinetic energy of rotating mass, P_e is the supplied power, and P_m is the driving mechanical power.

The main objective of the PCA is to control the rotor motion acceleration in terms of reducing the difference between $P_m - P_e$, as demonstrated in (23) and (24). Under the stable operation of the PMSM plant, while neglecting the losses, it can be written

$$P_e = P_m. \tag{25}$$

Hence, the rotor shaft acceleration of $d\omega_m/dt$ is zero. However, if a disturbance occurs in the torque or the desired change in speed, the plant goes out of a steady-state period. Therefore, PCA should gradually control the input of P_e until the PMSM plant returns to a stable operating state. Meanwhile, from (24), P_e depends on the rotor velocity and electromagnetic torque, which means that PCA can control P_e by modifying the reference velocity ($\omega_{\rm ref}$). The reduction of the ($P_m - P_e$) difference by controlling the reference velocity is indirectly related to the control of the manipulated variables of the reference voltages of the *d-q* axes for the proposed cost function. Since the reference voltages are indirectly proportional to the reference velocity, P_e is also affected by the reference voltages as shown in (8), (18), (19), and (24). Therefore, the PCA will replace the demand reference velocity with the modified reference velocity at every prediction time to reduce the ($P_m - P_e$) difference and thus control the rotor motion acceleration. The two procedures described below illustrate how the PCA calculates the modified reference velocity ($\omega_{d\text{-ref}}$).

1) Procedure #1: At every prediction time, the reference velocity is adjusted to reduce the difference and the measured velocity such as

$$\omega_{d-\rm ref} = (\omega_{\rm ref} + \omega_m)/2 \tag{26}$$

where $\omega_{d\text{-ref}}$ is the modified reference velocity. Thus, $\omega_{d\text{-ref}}$ will be set as the reference velocity of the proposed cost function instead of $\omega_{\rm ref}$. This step aims to select the appropriate reference voltages to easily stop the shaft acceleration if needed. Besides, PCA enables the computation of (26) until the absolute difference ($\omega_{\rm ref} - \omega_m$) is less than or equal to a small value of z_1 at about 2 r/min. Otherwise, the motor speed would fluctuate. Besides, the absolute reference velocity should be less than the absolute measured velocity. If (26) is not considered from the start, the proposed MPC algorithm will give large reference voltages, resulting in a large difference of ($P_{\rm m} - P_{\rm e}$). Thus, the proposed MPC loses control of the rotor motion acceleration as illustrated above.

2) Procedure #2: When the ($\omega_{\rm ref} - \omega_m$) difference is small, the modified reference velocity ($\omega_{d\text{-ref}}$) will be adjusted again, for a faster transition to the steady-state period without speed oscillations, depending on the measured velocity and the maximum velocity in the constant torque region ($\omega_{\rm max\text{-}CT}$) as defined as

$$\omega_{d-\rm ref} = \frac{|\omega_{d-\rm ref}|}{\omega_{d-\rm ref}}|\omega_m| - z_4 c_1 \omega_{\rm max-CT} \tag{27}$$

where c_1 is a factor to convert the revolution per minute to radian per second, and z_4 is the factor of 0.2 r/min. Meanwhile, z_4 is set to obtain a portion of the maximum velocity of the constant-torque region ($\omega_{\rm max\text{-}CT}$) for the controlled motor. Besides, $\omega_{\rm max\text{-}CT}$ can be represented as shown by

$$\omega_{\rm max-CT} = V_{\rm dc}/\left(\sqrt{3}\lambda_m C_e\right) \tag{28}$$

where C_e is the motor voltage coefficient. The purpose of procedure (27) is to eliminate the steady-state error of the velocity. However, it has a constraint to check that $\omega_{d\text{-ref}}$ is neither too close nor too far from ω_m. The constraint is that the difference of ($|\omega_m|$–$|\omega_{d\text{-ref}}|$) is greater than $c_1 z_2$ and less than $c_1 z_3$. Therefore, z_2 and z_3 can be defined to determine if this difference is small or large by 0.2 r/min and 16 r/min, respectively. Finally, Fig. 2 depicts a flowchart showing how to calculate $\omega_{d\text{-ref}}$ at each time step of the proposed cost function for the prediction with the reference voltages.

PCA algorithm also calculates the reference stator current of the *d*-axis ($i_{ds\text{-ref}}$) while the motor is running in the flux-weakening region, which can be written as

$$\begin{cases} \text{if } |\omega_{d-\rm ref}| > |\omega_{\rm max-CT}| \\ \text{then } i_{ds-\rm ref} = (-\lambda_m/L_{ds}) + (V_{\rm dc}/(\sqrt{3}L_{ds}C_e|\omega_{d-\rm ref}|)) \end{cases}. \tag{29}$$

However, if $\omega_{d\text{-ref}}$ is detected in the region of constant torque, then $i_{ds\text{-ref}}$ can be defined as

$$\text{if } |\omega_{d-\rm ref}| \le |\omega_{\rm max-CT}| \text{ then } i_{ds-\rm ref} = 0. \tag{30}$$

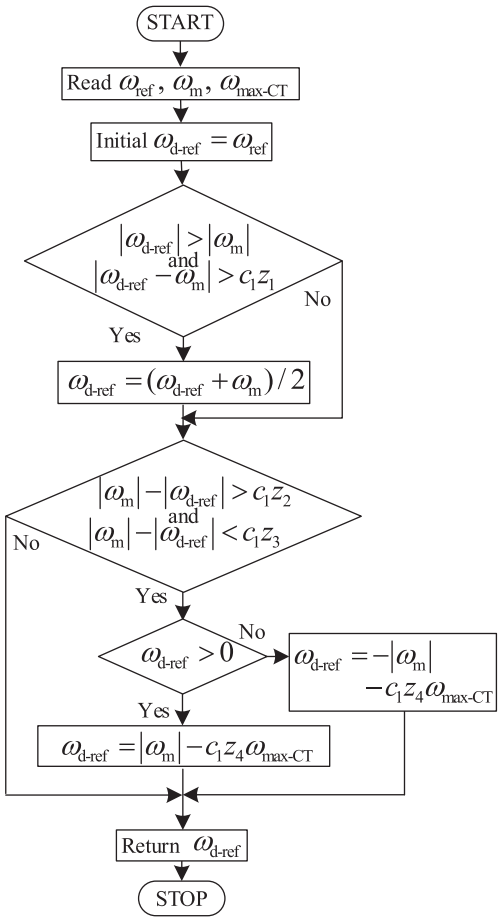

Fig. 2. Flowchart to compute the modified reference velocity.

For a further constraint, it is not decent for the motor current to get the maximum limit of the stator current ($I_{s\text{-max}}$) that the inverter can bear under obtaining the shortest settling time. Thus, PCA can propose a new constraint on the proposed cost function to reduce the overcurrent, which can be determined by the maximum limit of the drawn stator current ($I_{S\text{-}p\text{-max}}$). Also, this constraint is regarded as an indirect constraint on the shaft acceleration because of the required drawn current controls in P_e. Thus, the magnitude of the maximum limit current to be drawn by the motor can be determined in both the operating regions of the constant-torque and the flux-weakening as described by

$$\begin{cases} \text{if } |\omega_{d-\text{ref}}| > |\omega_{\max-\text{CT}}| \text{ then } I_{S-p-\max} = |i_{ds-\text{ref}}| + I_L \\ \text{if } |\omega_{d-\text{ref}}| \le |\omega_{\max-\text{CT}}| \text{ then } I_{S-p-\max} = I_{\text{rated}} \end{cases} \tag{31}$$

where I_{rated} is the rated current of PMSM, and I_L can be defined as

$$I_L = \delta T_L/(1.5 n_p \lambda_m). \tag{32}$$

Finally, the next section will show this constraint on the proposed fitness function.

D. Proposed Fitness Function

The objective function is one of the most important aspects of the MPC algorithm to adjust the motor performance for the next instant of (k+1). In this article, the objective function is proposed as

$$\text{Minimum } \{W_{id} |i_{ds-\text{ref}} - i_{ds-p}| + W_{wm} |\omega_{d-\text{ref}} - \omega_{m-p}|\}. \tag{33}$$

Meanwhile, the constraints of this objective function are given by

$$\begin{cases} \sqrt{(\delta V_{ds-\text{ref}})^2 + (\delta V_{qs-\text{ref}})^2} \le (V_{\text{dc}}/\sqrt{3}) \\ \sqrt{(i_{ds-p})^2 + (i_{qs-p})^2} \le I_{S-p-\max} \end{cases} \tag{34}$$

where $\omega_{m\text{-}p}$, $i_{ds\text{-}p}$, and $i_{qs\text{-}p}$ are the predicted motor velocity and the predicted stator currents of the d-q axes during the next sample time, W_{id} and W_{wm} are the weighting factors of current and velocity, $\delta V_{ds\text{-ref}}$ and $\delta V_{qs\text{-ref}}$ are the manipulated variables of the reference voltages of the d-q axes that will be prepared for the modulator, respectively. Meanwhile, the proposed cost function indirectly considers the predicted stator current for the q-axis depending on the further constraint (34). Besides, the proposed cost function straight fits the error of the motor speed to get high tracking performance, as can be seen from (33). Meanwhile, the improved reference speed is used as a demanded speed. Besides, the predicted values can be computed depending on the adaptive ADLPM for each iteration to search the optimal $\delta V_{ds\text{-ref}}$ and $\delta V_{qs\text{-ref}}$ for minimizing (33) by an MPC optimizer. Thus, the predicted values of $\omega_{m\text{-}p}$, $i_{ds\text{-}p}$, and $i_{qs\text{-}p}$ are determined by

$$\begin{vmatrix} i_{ds-p}[k+1] \\ i_{qs-p}[k+1] \\ \omega_{m-p}[k+1] \end{vmatrix} = \begin{vmatrix} \delta i_{ds}[k+1] \\ \delta i_{qs}[k+1] \\ \delta \omega_m[k+1] \end{vmatrix} = A_d[k] \begin{vmatrix} \delta i_{ds}[k] \\ \delta i_{qs}[k] \\ \delta \omega_m[k] \end{vmatrix} + B_d[k] \begin{vmatrix} \delta V_{ds-\text{ref}}[k] \\ \delta V_{qs-\text{ref}}[k] \end{vmatrix} + E_d[k]\, \delta T_L[k]. \tag{35}$$

Regarding the adjustment of the weighting factors, in the operation of the flux-weakening region, the error of the d-axis reference stator current should be reduced to achieve the desired velocity. Therefore, W_{id} would be greater than W_{wm} through this region as shown by

$$\text{if } |\omega_{\max-\text{CT}}| < |\omega_{F-\text{ref}}| \text{ then } W_{id} = 1, W_{wm} = 0.5. \tag{36}$$

Otherwise, W_{id} and W_{wm} can be defined as

$$W_{id} = 0.2, W_{wm} = 1. \tag{37}$$

IV. Simulation and Analysis

Comprehensive simulation and analysis of the PMSM drive system based on the proposed MPC, traditional FOC, and classical MPC strategies are fully performed using MATLAB/Simulink [12], [25]. Furthermore, the flowchart as depicted in Fig. 3 shows the main steps for the proposed MPC implementation. Besides, the offline identification values of the nominal machine parameters for the PMSM and voltage inverter, at the temperature of 20 °C, are listed in Table I. For determining

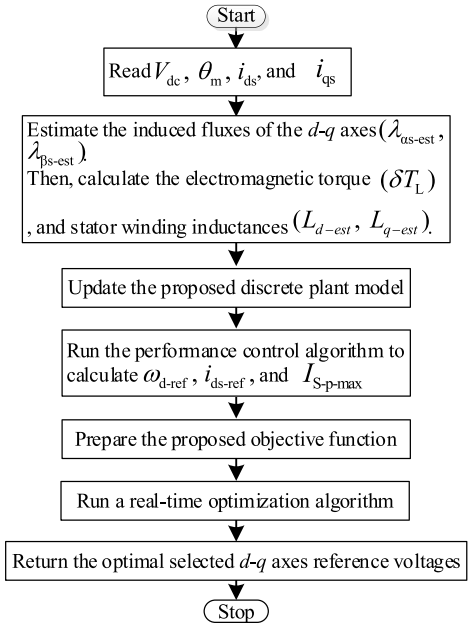

Fig. 3. Flowchart of the proposed MPC.

TABLE I
MAIN PARAMETERS OF THE PROPOSED INTERIOR PMSM DRIVE

Parameters	Symbols	Quantities	Units
Rated velocity	ω_r	209.4	rad/s
Rated current	I_{rated}	6	A
Rated torque	T_r	14	Nm
Rated power	P_r	3	kW
Stator resistance	R_s	1.14	Ω
Stator d-axis inductance	L_d	1.91e-3	H
Stator q-axis inductance	L_q	4.73e-3	H
Permanent magnet flux linkage	λ_m	0.38	Wb
Moment of inertia	J	3.78e-4	Kg.m^2
Viscous coefficient	B_v	7.403e-5	-
Number pole pairs	n_p	3	-
DC-link voltage	V_{dc}	450	V
Motor voltage constant	C_e	3.2035	-
Constant switching frequency	F_{sw}	2.5	kHz
Inverter maximum current	$I_{s\text{-}max}$	20	A
Time step	T_s	0.0001	s

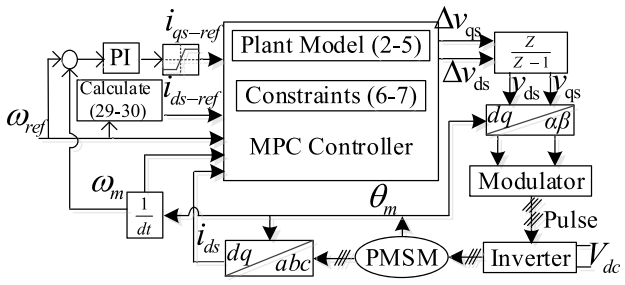

Fig. 4. Block diagram of the classical MPC algorithm.

the d-axis current under the classical MPC, it is calculated by (29) and (30) during the flux weakening range. Finally, the block diagram of the classic MPC is shown in Fig. 4, where $i_{qs\text{-}ref}$ is the reference stator current of the q-axis. Meanwhile, the proposed MPC algorithm makes predictions about the future output and the optimizer finds the best sequence of the control

TABLE II
MAIN DIFFERENCES BETWEEN THE PROPOSED AND TRADITIONAL MPCS

	Proposed MPC	Traditional MPC
The predictive model considers the induced torque that …	can be adaptive.	must be known in advance as a constant.
The machine parameters of the predictive model …	can be adaptive.	are constant.
The state vector of a predictive model has …	three components.	seven components.
The performance control algorithm is based on …	clear and definite coefficients.	approximate rate factor.

voltages that drives the predicted outputs as close to the reference points as possible. Thus, a prediction horizon that will cover the significant dynamics of the proposed driving system should be chosen. The recommendation for choosing the prediction horizon is to have 20 to 30 samples covering the open-loop response of the proposed system. Besides, the control horizon is set to 10% to 20% of the prediction horizon to avoid heavy computation and to obtain better prediction [33], [34]. Therefore, the prediction and control horizons of the MPC algorithms are 10 and 3, respectively.

A performance comparison is presented between the proposed MPC strategy and the FOC strategy in [12] to prove the effectiveness of the proposed MPC strategy. For a fair comparison, all modifications in [12] are considered to improve the dynamic performance of the FOC strategy. According to these modifications, the gains of the PI controllers are adjusted depending on the offline optimization procedure as explained in [12]. Meanwhile, the techniques of the anti-windup and decoupling feedforward are employed to reduce the signal overshoot. Besides, the plant model and the constraint of the overspeed for the classical MPC strategy as presented in [25] serve as a benchmark to highlight the better performance of the proposed MPC strategy when compared to each other. Thus, key differences between the proposed and traditional MPC strategies are given out in Table II.

A. Dynamic Performance of Sudden Changes in Speed and Torque

In this section, the velocity of the PMSM is fully analyzed in both operation regions. Besides, the motor is tested upon sudden change of initial load torque in the constant power region. Therefore, Figs. 5–7 show the performance of the PMSM under the proposed MPC, the classical MPC, and the FOC, separately. For the scenario of these figures, the reference velocity is about 235.62 rad/s under the initial load of 0.5 N·m which suddenly increases to 4 N·m. Finally, the reference velocity will drop abruptly from the flux-weakening region to about 188.5 rad/s in the constant torque region.

Figs. 5(a), 6(a), and 7(a) show the measured velocity, reference velocity, and modified reference velocity of the proposed MPC, conventional MPC, and the FOC, respectively. It should

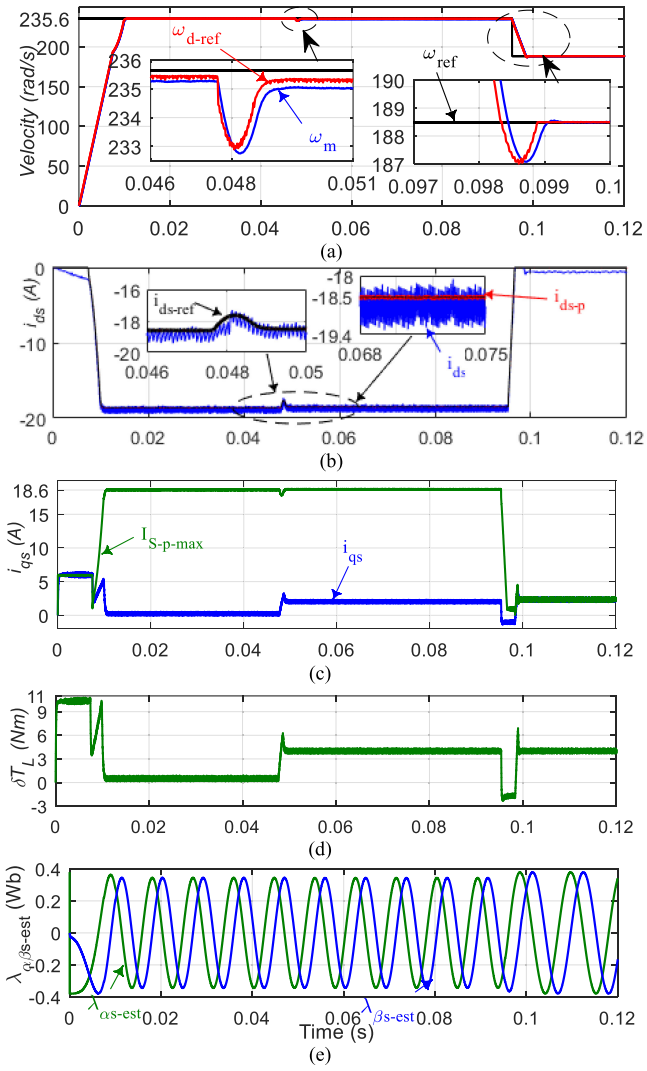

Fig. 5. Simulation performance of the proposed MPC strategy where (a) measured, original reference, and modified reference velocities (ω_m, $\omega_{\rm ref}$, and $\omega_{d\text{-ref}}$), (b) measured and reference d-axis currents (i_{ds}, and $i_{ds\text{-ref}}$), (c) q-axis current (i_{qs}), (d) estimated torque (δT_L), and (e) α-β axes estimated fluxes ($\lambda_{\alpha s\text{-est}}$ and $\lambda_{\beta s\text{-est}}$).

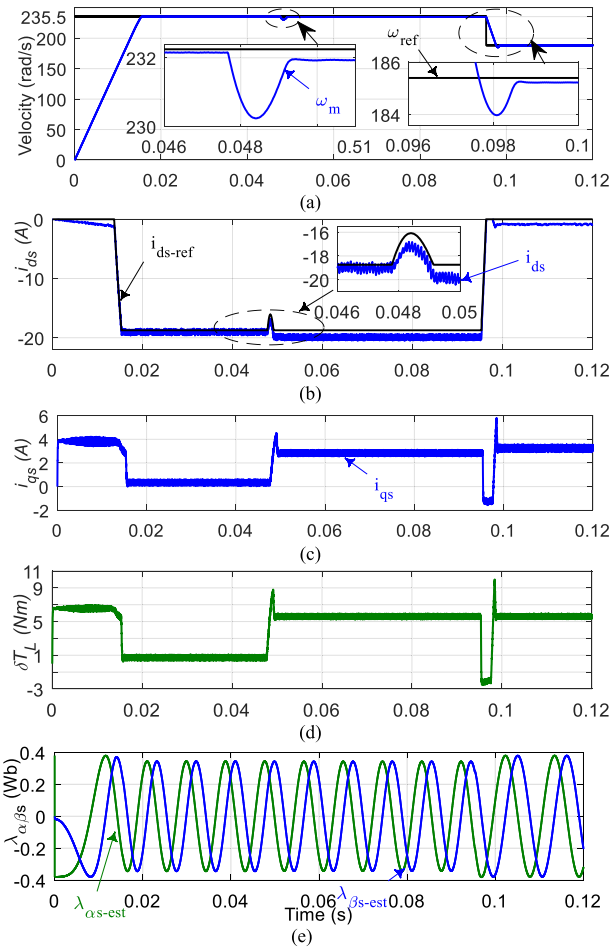

Fig. 6. Simulation performance of the traditional MPC strategy where (a) measured, and original reference motor velocities (ω_m and $\omega_{\rm ref}$), (b) measured and reference d-axis currents (i_{ds} and $i_{ds\text{-ref}}$), (c) q-axis current (i_{qs}), (d) estimated torque ($\delta T_{\rm L}$), and (e) α-β axes estimated fluxes ($\lambda_{\alpha s\text{-est}}$ and $\lambda_{\beta s\text{-est}}$).

be mentioned that the reference velocity is modeled as a step signal in all three implemented strategies.

However, the proposed MPC algorithm is based on the modified reference velocity provided by the proposed PCA rather than the original reference velocity. As shown in Fig. 5(a), the modified reference velocity appears as a function of a slope. Therefore, it can be seen from these figures that the settling time is reduced under the proposed MPC by about 34.1% relative to the classical MPC and about 73% relative to the FOC. This is the reason behind the time scale in Figs. 5 and 7 ranging from 0 to 0.12 s in Fig. 5 and 0 to 1 s in Fig. 7. Meanwhile, the speed drop during torque disturbance is reduced under the proposed MPC by about 43.8% relative to the classical MPC and about 85.1% relative to the FOC. Besides, the speed drop during velocity change is reduced under the proposed MPC by about 60.1% relative to the classical MPC and about 91.9% relative to the FOC. Finally, the steady-state error under the FOC is about 2 rad/s, and lower than 0.5 for both MPCs. As a result, the actual speeds cannot track the reference speed accurately for the following reasons. For the FOC strategy, the flux outer control loop can automatically adjust the flux level based on the reference duty cycle. However, this steady-state error is obtained due to the linearity of the proportional controller of the speed PI controller and the nonlinearity of the controlled PMSM plant. For the classical MPC strategy, the fixed parameters of the predictive model cause this steady-state error because the predictive model cannot accurately represent the nonlinearity of the controlled PMSM. Therefore, the proposed MPC has the most stable speed due to its shorter settling time and lower undershoot. Thus, the credit goes to the PCA, which can control the shaft acceleration more robustly than depending on the change rate of the reference voltages of the traditional MPC. Besides, the speed error directly controls the performance of the motor within the proposed cost function.

Figs. 5(b), 6(b), and 7(b) show the d-axis measured current, the computed reference current of the PCA, and the predicted current of the proposed MPC, conventional MPC, and the FOC, respectively. It can be seen from these figures that the mean value

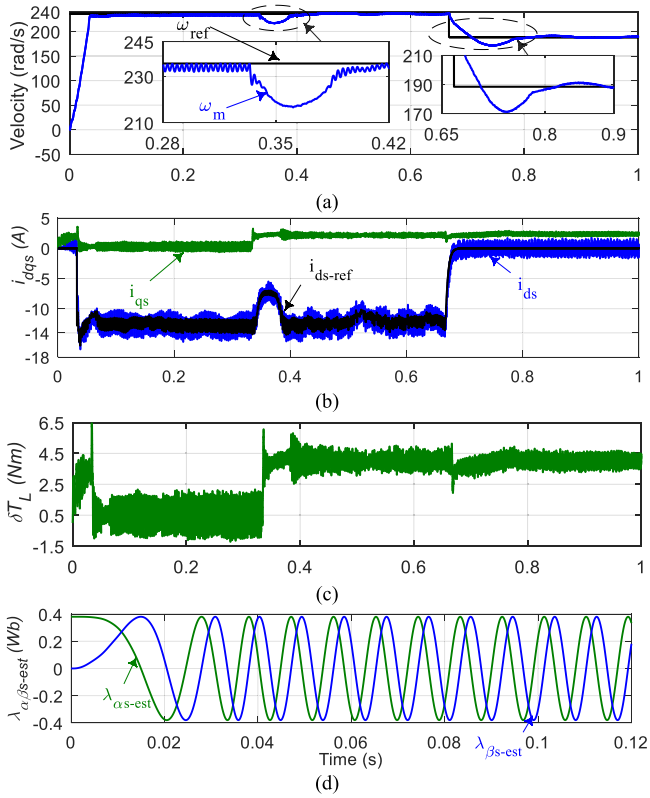

Fig. 7. Simulation performance of the FOC strategy where (a) motor velocity (ω_m), (b) d-q axes currents (i_{ds} and i_{qs}), (c) estimated electromagnetic torque ($\delta T_{\rm L}$), and (d) α-β axes estimated fluxes ($\lambda_{\alpha s\text{-est}}$ and $\lambda_{\beta s\text{-est}}$).

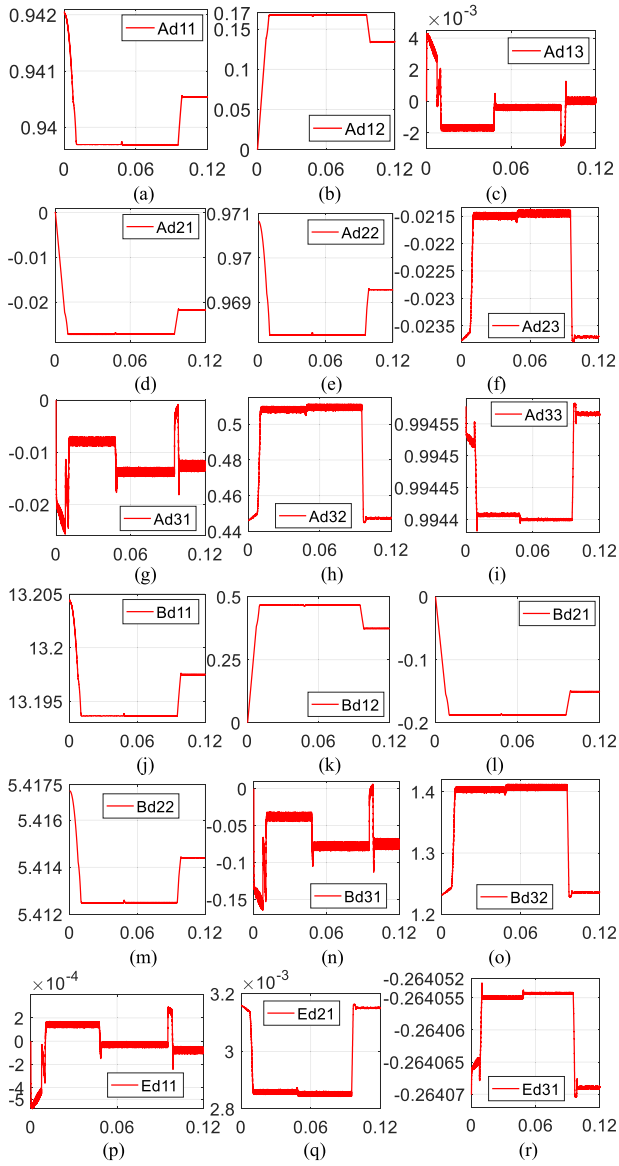

Fig. 8. Discretization matrices of the proposed MPC strategy where (a) $A_{\rm d11}$, (b) $A_{\rm d12}$, (c) $A_{\rm d13}$, (d) $A_{\rm d21}$, (e) $A_{\rm d22}$, (f) $A_{\rm d23}$, (g) $A_{\rm d31}$, (h) $A_{\rm d32}$, (i) $A_{\rm d33}$, (j) $B_{\rm d11}$, (k) $B_{\rm d12}$, (l) $B_{\rm d21}$, (m) $B_{\rm d22}$, (n) $B_{\rm d31}$, (o) $B_{\rm d32}$, (p) $E_{\rm d11}$, (q) $E_{\rm d21}$, and (r) $E_{\rm d31}$.

of the d-axis current under the proposed MPC, before and after the torque disturbance period, is reduced by about 1% and 2.6% relative to the classical MPC, respectively. Besides, the mean value of the traditional MPC current in the steady-state period will grow up negatively relative to the reference current while increasing the torque. Finally, the peak of the d-axis current ripple is reduced under the proposed MPC by about 1% relative to the classical MPC and about 78.7% relative to the FOC.

The performance of the stator current is controlled by the further constraint of $I_{S\text{-}p\text{-max}}$, as shown in Fig. 5(c). As a result, it can be seen from Figs. 5(c) and 6(c) that the q-axis current peak under the proposed MPC is controlled well within the range of the motor rated current ($I_{\rm rated}$) even though it is higher than that under the classical MPC during the transient period to reduce the transient time of speed. Meanwhile, there is a spike in the q-axis current attempting to grow up.

Thus, this reflects the significance of the constraint, $I_{S\text{-}p\text{-max}}$, in terms of breaking this spike at a portion of the transient time. As a result, the mean value of the q-axis current under the proposed MPC, before and after the torque disturbance period, is reduced by about 31% and 28% relative to the classical MPC and about 4% and 5.5% relative to the FOC, respectively. Finally, the peak of the q-axis current ripple is reduced under the proposed MPC by about 1.1% relative to the classical MPC and about 25% relative to the FOC.

Meanwhile, Figs. 5(d), 6(d), and 7(c) show the computed electromagnetic torque. As can be seen from these figures, the proposed MPC has the highest starting torque and can reduce the peak of torque ripple resulting from the fluctuation of the currents by about 1.4% and 54.7% relative to the classical MPC and the FOC, respectively. Thus, the FOC strategy needs to be further improved to enhance the performance of the interior-type PMSM [35]. Figs. 5(e), 6(e), and 7(d) show the estimated α-β axes fluxes relying on the TOGI observer for the proposed MPC, the classical MPC, and the FOC strategies, respectively. Thus, the ADLPM of the proposed MPC can consider the variable operating torque to reduce speed drop, as well as the ripple of current and torque.

The instantaneous values of the discretization matrices for $A_{\rm d}$, $B_{\rm d}$, and $E_{\rm d}$ are shown in Fig. 8 based on (14)–(17). As mentioned above, the purpose of these calculations is to update the internal ADLPM over each speed region to better represent

TABLE III
TRADITIONAL STRATEGIES PERFORMANCE RELATIVE TO THE PROPOSED MPC FOR THE SIMULATION STUDY

Items	Proposed MPC	Classical MPC	FOC
Settling time	0.0095 s	1.5 times	3.7 times
Speed drop rate (at torque disturbance)	2.9 rad/s	1.8 times	6.7 times
Speed drop rate (at velocity change)	2 rad/s	2.5 times	12.3 times
Steady-state error	0.0	0.5 rad/s	2 rad/s
Mean i_{ds}	−18.93 A	1.1 times	equal
i_{ds} ripple	0.5 A	1.1 times	4.7 times
Mean i_{qs} (before torque disturbance)	0.25 A	1.5 times	1.4 times
Mean i_{qs} (after torque disturbance)	2.03 A	1.1 times	1.1 times
i_{qs} ripple	0.27 A	1.1 times	1.4 times
Torque ripple	0.31 Nm	1.1 times	2.2 times

the PMSM plant. Finally, Table III summarizes the superiority of the performance of the proposed MPC compared to the classical MPC and FOC strategies for the simulation study.

B. Dynamic Performance of Variable Machine Parameters

This section presents the simulation dynamic results if the machine parameters differ under the same operating conditions of speed and torque as in the previous simulation study. Meanwhile, this section shows what extent the proposed MPC and classical MPC methods depend on those parameters. Thus, the stator resistance of the controlled PMSM is increased from the nominal value to 1.12 Ω at the temperature of 122 °C [12]. For the stator winding inductance, it will decrease by about 40% when magnetic saturation occurs [12].

Fig. 9(a)–(c) shows the motor velocity and stator currents of the *d*-*q* axes under the proposed MPC and classical MPC, respectively. Besides, matching the estimated rotor position to the counted rotor position proves the ability of the TOGI flux observer to provide machine parameters for the proposed MPC, as shown in Fig. 9(d) and (e), where the estimated rotor position ($\theta_{m\text{-est}}$) can be calculated as

$$\theta_{m-\text{est}} = a\tan 2\left(\frac{\lambda_{\beta s-\text{est}}}{\lambda_{\alpha s-\text{est}}}\right). \tag{38}$$

As a result, the online estimated values of stator inductances for the *d*-*q* axes of the proposed MPC and classical MPC are presented in Fig. 9(f) and (g), respectively. Finally, Table IV shows the effect of changing machine parameters on the proposed method and the classical method. Thus, it can be concluded from this table that the proposed adaptive MPC method is less dependent on changing machine parameters than the classical MPC method.

V. EXPERIMENTAL RESULTS AND DISCUSSIONS

Comprehensive experiments and analysis are carried out in this section to verify the proposed MPC in comparison to the FOC and traditional MPC strategies. Therefore, two scenarios

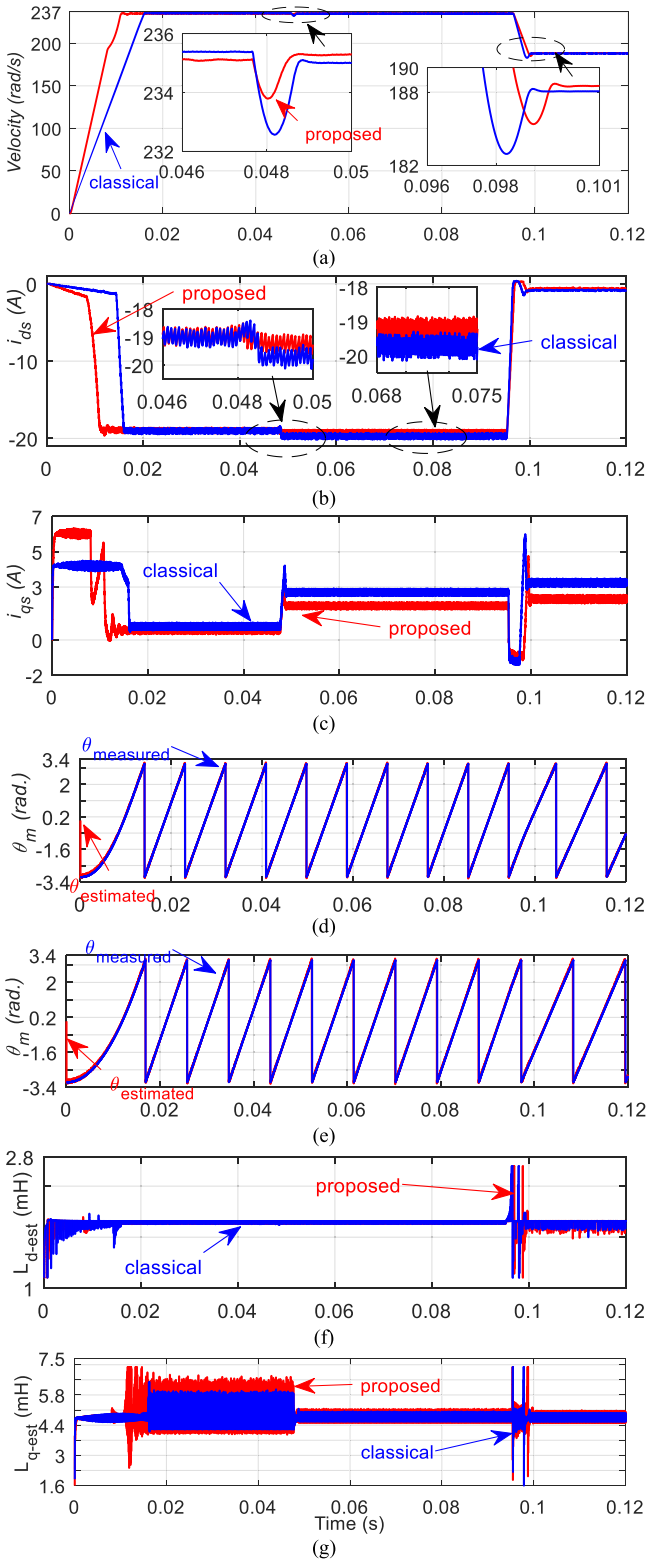

Fig. 9. Simulation results in the case of the changing machine parameters under the control of the proposed MPC and classical MPC where (a) measured velocities (ω_m), (b) measured *d*-axis current (i_{ds}), (c) measured *q*-axis current (i_{qs}), (d) estimated and measure rotor positions ($\theta_{m\text{-est}}$, θ_m) of the proposed MPC, (e) estimated and measure rotor positions ($\theta_{m\text{-est}}$, θ_m) of the classical MPC, (f) estimated *d*-axis inductance ($L_{d\text{-est}}$), and (g) estimated *q*-axis inductance ($L_{q\text{-est}}$).

TABLE IV
CLASSICAL MPC PERFORMANCE RELATIVE TO THE PROPOSED MPC FOR THE SIMULATION STUDY OF CHANGING MACHINE PARAMETERS

Items	Proposed MPC	Classical MPC
Settling time	0.01 s	1.5 times
Speed drop rate (at torque disturbance)	1.9 rad/s	1.7 times
Speed drop rate (at velocity change)	3.1 rad/s	1.8 times
Steady-state error	0.5 rad/s	2 times
Mean i_{ds} (after torque disturbance)	−19.2 A	1.1 times
i_{ds} ripple (after torque disturbance)	0.35 A	1.1 times
Mean i_{qs} (after velocity change)	2.3 A	1.5 times

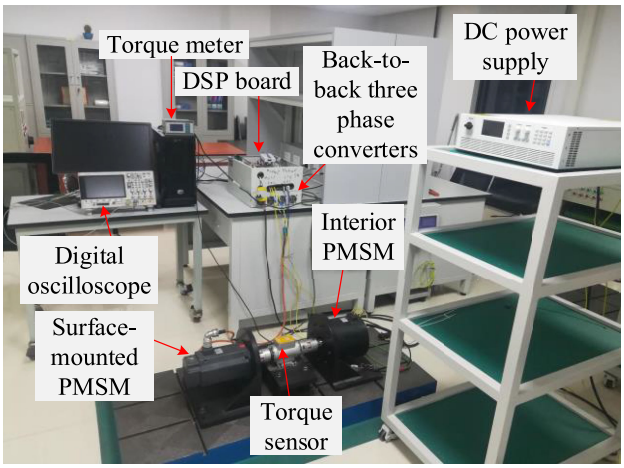

Fig. 10. Experimental setup.

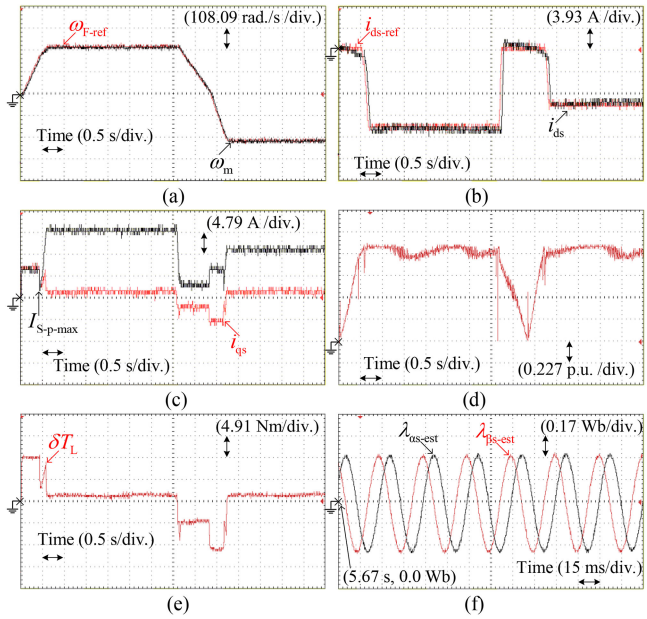

Fig. 11. Experimental results of the proposed MPC strategy in case of four-quadrant control where (a) motor measured velocity and manipulated modified reference velocity (ω_m, $\omega_{d\text{-ref}}$), (b) d-axis measured current, and reference current (i_{ds}, $i_{ds\text{-ref}}$), (c) q-axis measured current and maximum magnitude of the stator current (i_{qs}, $I_{S\text{-}P\text{-max}}$), (d) estimated electromagnetic torque (δT_{L}), (e) α-β axes estimated fluxes ($\lambda_{\alpha s\text{-est}}$, $\lambda_{\beta s\text{-est}}$), and (f) voltage vector (ρ).

are given out in the laboratory relying on the floating-point digital signal processor controller of DSP28335, as shown in Fig. 10. In this setup, a surface-mounted PMSM of 3 kW serves as the controlled load and is coupled to the primary PMSM. Also, the encoder of 4096 pulses per cycle is used to calculate the mechanical angle. Finally, the proposed MPC execution time is 0.1 s due to the computational burden of the real-time optimization procedure [28], [29].

A. Dynamic Performance of Four-Quadrant Control Study

In this section, the four-quadrant operation of the controlled PMSM is examined while the motor is operating in both regions at the constant torque and the flux weakening. For the scenario of this case, the reference velocity is 230.4 rad/s, and the initial load torque is about 1.5 N·m. Afterward, the reference velocity abruptly reverses to −225.2 rad/s. Thus, Figs. 11–13 show the dynamic performance of the PMSM drive under the proposed MPC, traditional MPC, and FOC strategies, respectively.

In Fig. 11(a), the reference velocity (ω_{ref}) is programmed as a step signal and not a slope signal. However, the proposed MPC algorithm is based on the modified reference velocity by the proposed PCA rather than the original reference velocity. As a result, the modified reference velocity appears as a function of a slope. Besides, the measured velocity under the proposed MPC has a settling time of about 0.55 s and no over speed.

Meanwhile, the settling time is reduced by about 30.7% relative to the conventional MPC and about 86.6% relative to the FOC strategy, as shown in Figs. 11(a), 12(a), and 13(a), respectively. Besides, it can be seen from these figures that the proposed MPC velocity has shifted quickly and smoothly from the forward direction to the reverse direction, along with regions of constant torque and constant power. Furthermore, it is noticeable that the velocity of the FOC strategy has a delay in response to the reverse direction, as well as a steady-state error of about 13.6 rad/s. Thus, this indicates that the FOC strategy is unable to establish the connection between the speed controller and the field-weakening controller.

Figs. 11(b), 12(b), and 13(b) show the d-axis measured current and d-axis computed reference current of the proposed MPC, traditional MPC, and the FOC strategy, respectively. For the operation in the flux-weakening region, the mean d-axis current is reduced by about 1.7% under the proposed MPC relative to the classical MPC. Meanwhile, the proposed MPC can reduce the peak of the d-axis current ripple by about 2.3% relative to the classical MPC and about 82.7% relative to the FOC. Besides, the mean value of the d-axis current of both MPCs is the same in the reverse direction of about −10 A. However, the d-axis current of classic MPC does not follow the reference at the steady-state region. The reason for this is that the linear model plant for the classical MPC has a previously known constant torque value that does not properly express the system torque.

Besides, the further constraint of the $I_{S\text{-}P\text{-max}}$ of the PCA reduces the mean value of the q-axis current. As a result, it

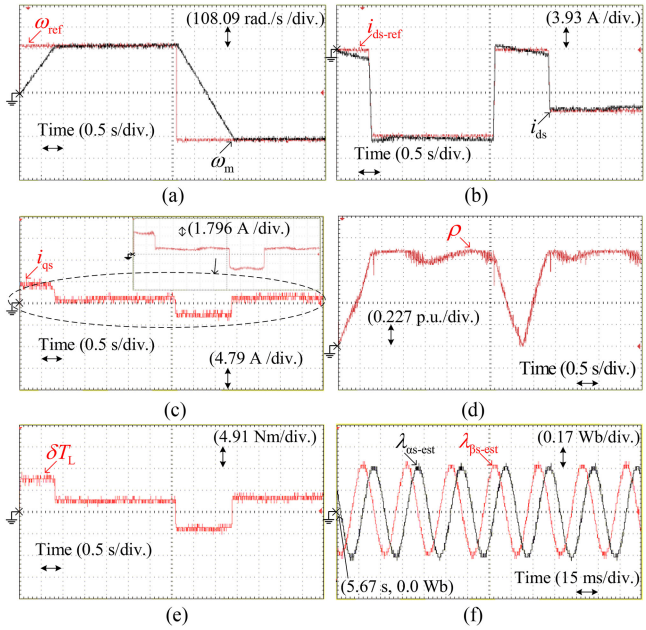

Fig. 12. Experimental results of the conventional MPC strategy in the case of four-quadrant control where (a) motor measured velocity and reference velocity (ω_m, $\omega_{\rm ref}$), (b) d-axis measured current, and reference current (i_{ds}, $i_{ds\text{-ref}}$), (c) q-axis measured current (i_{qs}), (d) voltage vector (ρ), (e) estimated electromagnetic torque (δT_L), and (f) α-β axes estimated fluxes ($\lambda_{\alpha s\text{-est}}$, $\lambda_{\beta s\text{-est}}$).

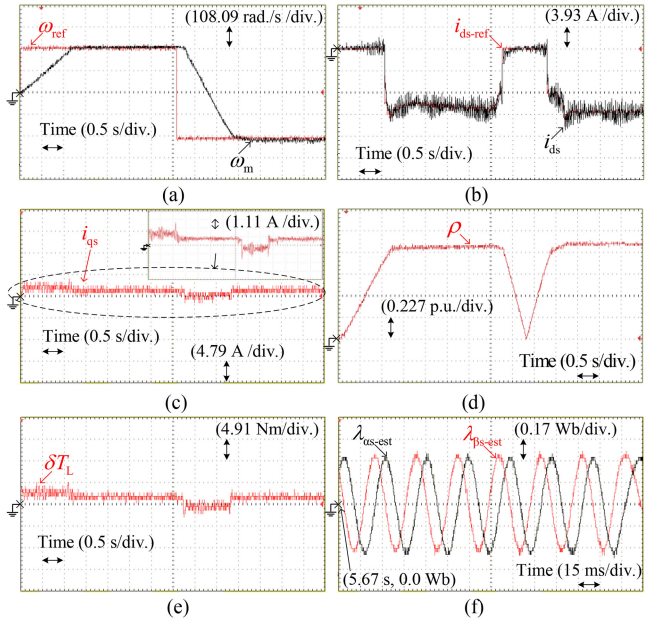

Fig. 13. Experimental results of the FOC strategy in case of four-quadrant control where (a) motor measured velocity and reference velocity (ω_m and $\omega_{\rm ref}$), (b) d-axis measured current (i_{ds}), and d-axis reference current, (c) q-axis measured current (i_{qs}), (d) voltage vector (ρ), (e) estimated electromagnetic torque (δT_L), and (f) α-β axes estimated fluxes ($\lambda_{\alpha s\text{-est}}$, $\lambda_{\beta s\text{-est}}$).

can be seen from Figs. 11(c), 12(c), and 13(c) that the mean q-axis current is reduced by about 28.5% under the proposed MPC relative to the classical MPC and about 9.2% relative to the FOC. Besides, the wave of the q-axis current contains a peak that is attempting to increase in height. As a result, it reflects the significance of the constraint ($I_{S\text{-}P\text{-max}}$) in terms of breaking this increase in the transient period. Meanwhile, the proposed MPC can reduce the peak of the q-axis current ripple by about 2.4% relative to the classical MPC and about 27.7% relative to the FOC.

The calculated torque and estimated α-β axes fluxes for the proposed MPC, the traditional MPC, and the FOC strategy are presented in Figs. 11(d) and (e), 12(e) and (f), and 13(e), and (f). Thus, the proposed MPC can also adapt the variable load torque in the internal ADLPM to obtain high performance in each speed region based on increasing the predicting efficiency of the state variables to select the appropriate reference voltage of the d-q axes. Therefore, the proposed MPC can reduce the peak of the torque ripple by about 6.1% relative to the classical MPC and about 53.2% relative to the FOC.

The voltage trajectory (ρ) can be defined to determine the maximum limit of $0.0578V_{\rm dc}$ that the inverter can supply to the motor, as presented in Figs. 11(f), 12(d), and 13(d), where the base voltage is 450 V, and ρ can be defined as

$$\rho = \sqrt{V_{ds-\rm ref}^2 + V_{qs-\rm ref}^2}/V_{\rm dc}. \tag{39}$$

Therefore, the voltage vectors are in the region of the flux-weakening, where they are close to unity. Finally, Table V summarizes the superiority of the performance of the proposed MPC compared to the classical MPC and FOC strategies for the four-quadrant control study.

TABLE V
TRADITIONAL STRATEGIES PERFORMANCE RELATIVE TO THE PROPOSED MPC FOR THE FOUR-QUADRANT CONTROL STUDY

Items	Proposed MPC	Classical MPC	FOC
Settling time	0.55 s	1.5 times	7.4 times
Steady-state error	0.0	0.0 rad/s	13.6 rad/s
Mean $i_{\rm ds}$ (before speed variation)	−14.8 A	1.1 times	equal
Mean $i_{\rm ds}$ (after speed variation)	−10 A	1.1 times	equal
$i_{\rm ds}$ ripple	0.4 A	1.1 times	5.7 times
Mean $i_{\rm qs}$	0.8 A	1.4 times	1.1 times
$i_{\rm qs}$ ripple	0.25 A	1.1 times	1.4 times
Torque ripple	0.32 Nm	1.1 times	2.2 times

B. Dynamic Performance in Case of the Parameters Mismatching of Stator Winding Inductances

This section presents the experimentally dynamic results if the stator inductance parameters of the predictive models of the proposed and classical MPC methods do not match the nominal parameters listed in Table I which are reduced by 20%. Meanwhile, the four-quadrant operation of the PMSM controlled system is also investigated with the same operating conditions for speed and torque as in the previous experimental study. Thus, this section shows to what extent the proposed and classical MPC algorithms depend on those parameters.

Figs. 14(a)–(c) and 15(a)–(c) show the motor velocity and stator currents of the d-q axes under the proposed MPC and

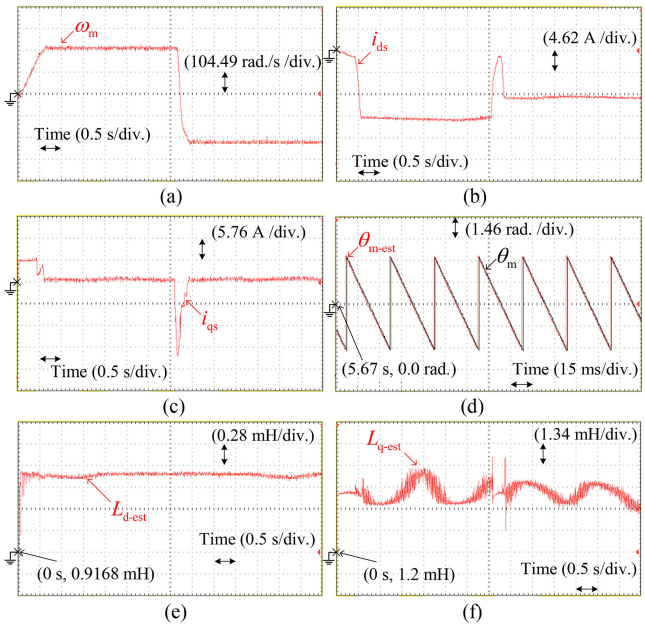

Fig. 14. Experimental results of the proposed MPC strategy in the case of the parameters mismatching where (a) motor measured velocity (ω_m), (b) d-axis measured current (i_{ds}), (c) q-axis measured current (i_{qs}), (d) estimated and measure rotor positions ($\theta_{m\text{-est}}$, θ_m), (e) estimated d-axis inductance ($L_{d\text{-est}}$), and (f) estimated q-axis inductance ($L_{q\text{-est}}$).

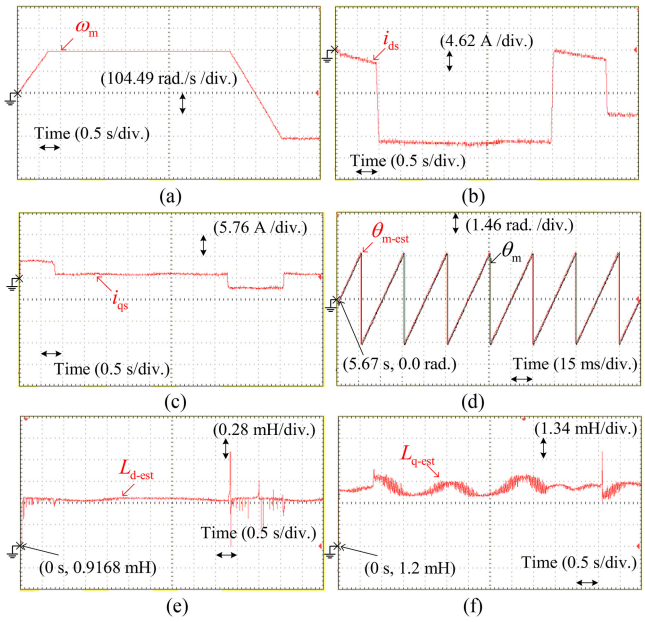

Fig. 15. Experimental results of the classical MPC strategy in the case of the parameters mismatching where (a) motor measured velocity (ω_m), (b) d-axis measured current (i_{ds}), (c) q-axis measured current (i_{qs}), (d) estimated and measure rotor positions ($\theta_{m\text{-est}}$, θ_m), (e) estimated d-axis inductance ($L_{d\text{-est}}$), and (f) estimated q-axis inductance ($L_{q\text{-est}}$).

classical MPC, respectively. Besides, matching the estimated rotor position to the counted rotor position proves the ability of the TOGI flux observer to provide machine parameters for the proposed MPC, as shown in Figs. 14(d) and 15(d). As a result, the online estimated values of stator inductances for the d-q axes of the proposed MPC and classical MPC are presented

TABLE VI
CLASSICAL MPC PERFORMANCE RELATIVE TO THE PROPOSED MPC OF PARAMETERS MISMATCHING CASE

Items	Proposed MPC	Classical MPC
Settling time (before speed variation)	0.5 s	1.5 times
Settling time (after speed variation)	0.3 s	10.9 times
Mean i_{ds} (before speed variation)	−14.81 A	1.3 times
Mean i_{ds} (after speed variation)	−10.24 A	1.3 times
Mean i_{qs} (before speed variation)	0.7 A	1.3 times

in Figs. 14(e) and (f) and 15(e) and (f), respectively. Finally, Table VI shows the effect of parameter mismatching on the proposed method and the classical method. Thus, it can be concluded from this table that the proposed MPC strategy is less dependent on mismatched parameters relative to the classical MPC strategy. The reason behind that the proposed MPC can adapt the parameters of the predictive model and the PCA. However, both the predictive model and flux-weakening current of (29) for the classical MPC strategy depend on the mismatched parameters.

C. Dynamic Performance of Velocity Oscillation and Load Torque Disturbance

Since the mechanical load and motor control would cause speed oscillation [13], this section will check the robustness of the proposed MPC in the case of velocity oscillation compared to the classical MPC and the FOC strategies.

For the scenario of this case, the PMSM is controlled to a reference velocity of 225.2 rad/s with an initial load torque of 0.5 N·m, then the load torque is suddenly increased to 7.5 N·m. Therefore, Figs. 16–18 show the dynamic performance of the drive system according to the control of the proposed MPC, traditional MPC, and the FOC strategies, separately.

As shown in Figs. 16(a), 17(a), and 18(a), the steady-state error of the proposed MPC, the classical MPC, and the FOC strategy is about 0.2%, 0.2%, and 2.2%, respectively. Also, it should be mentioned that the reference velocity is modeled as a step signal in all three implemented strategies. However, the proposed MPC algorithm is based on the modified reference velocity provided by the proposed PCA rather than the original reference velocity. As shown in Fig. 16(a), the modified reference velocity appears as a function of a slope. Thus, the settling time is reduced under the proposed MPC by about 39% relative to the classical MPC and about 76.8% relative to the FOC. Besides, the speed drop is reduced under the proposed MPC by about 29.9% relative to the classical MPC and about 65.1% relative to the FOC. As a result, it can be concluded that the proposed MPC strategy can track the reference velocity with the lowest steady-state error and smaller speed fluctuation. Besides, the performance of the FOC is the worst because it is not able to consider the required performance restrictions of the state variables altogether in one controller. Therefore, the

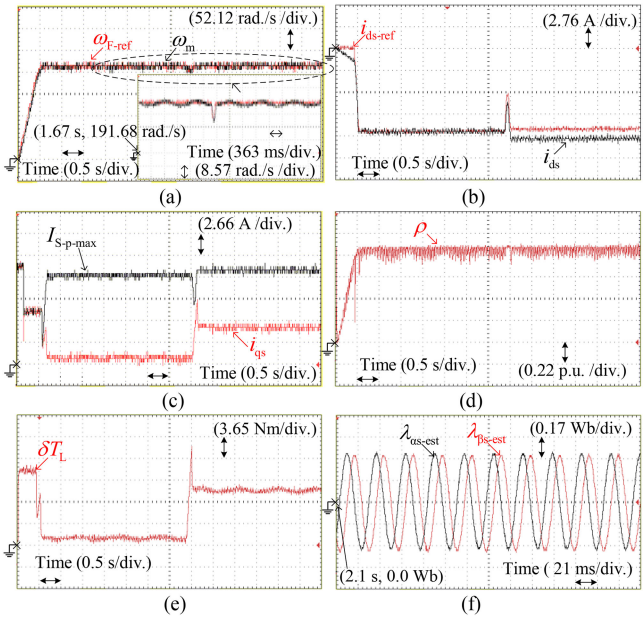

Fig. 16. Experimental results of the proposed MPC strategy for the oscillation speed condition and torque disturbance where (a) motor measured velocity and manipulated modified reference velocity (ω_m, $\omega_{\text{d-ref}}$), (b) d-axis measured current, and reference current (i_{ds}, $i_{ds\text{-ref}}$), (c) q-axis measured current and maximum magnitude of the stator current (i_{qs}, $I_{S\text{-}P\text{-max}}$), (d) estimated electromagnetic torque (δT_{L}), (e) estimated fluxes ($\lambda_{\alpha s\text{-est}}$, $\lambda_{\beta s\text{-est}}$), and (f) voltage vector (ρ).

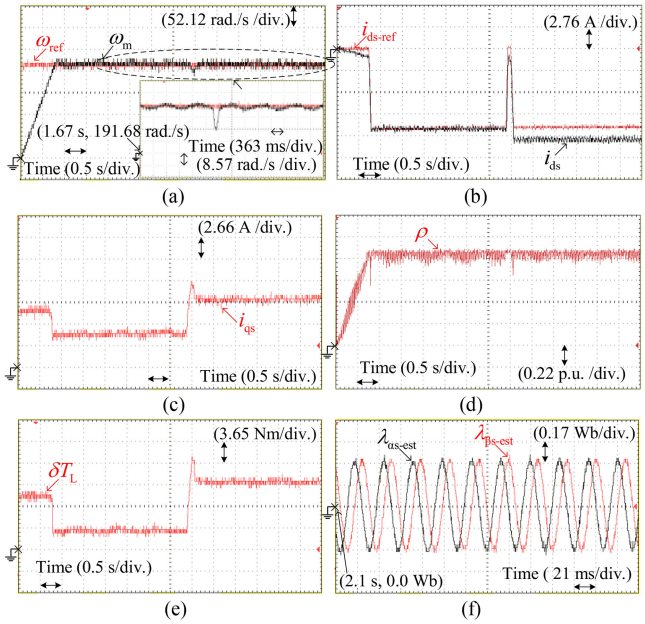

Fig. 17. Experimental results of the conventional MPC strategy for the oscillation speed condition and torque disturbance where (a) motor measured velocity and reference velocity (ω_m, ω_{ref}), (b) d-axis measured current, and reference current (i_{ds}, $i_{ds\text{-ref}}$), (c) q-axis measured current (i_{qs}), (d) voltage vector (ρ), (e) estimated electromagnetic torque (δT_L), and (f) estimated fluxes ($\lambda_{\alpha s\text{-est}}$, $\lambda_{\beta s\text{-est}}$).

interior type PMSM needs further modification based on the FOC strategy to get high performance [35].

Figs. 16(b), 17(b), and 18(b) show the d-axis measured current (i_{ds}), the computed reference current ($i_{ds\text{-ref}}$) of the PCA, and the predicted current ($i_{ds\text{-}p}$) of the proposed MPC, conventional MPC, and the FOC, respectively. It can be seen from these figures that the mean value of the d-axis current is reduced under the proposed MPC by about 0.52% relative to the classical MPC. However, the mean value of the classical MPC increases significantly in the negative trajectory due to the rising load torque. Meanwhile, the peak of the d-axis current ripple is reduced under the proposed MPC by about 3.7% relative to the classical MPC and about 80.1% relative to the FOC. Besides, the d-axis currents of the classical MPC and the FOC are cut to zero when the load torque is suddenly disturbed, which means that the speed tracking performance of these strategies is negatively affected. On the contrary, the PCA can keep the d-axis current in the negative trajectory to get high-speed tracking performance.

Figs. 16(c), 17(c), and 18(c) show the q-axis measured current (i_{ds}) of the proposed MPC, the classical MPC, and the FOC, respectively. It can be seen from these figures that the peak of the q-axis current ripple is reduced under the proposed MPC by about 2.4% relative to the classical MPC. The reason behind this is the used constant value of the torque of the classical MPC does not describe the actual variable torque. Meanwhile, the mean value of the q-axis current is reduced under the proposed MPC by about 21.2% relative to the classical MPC and about 11.4% relative to the FOC. Therefore, the calculation of $I_{\text{S-p-max}}$, as illustrated in Fig. 16(c), is a significant constraint for solving the proposed cost function rather than determining the rate of change of reference voltages.

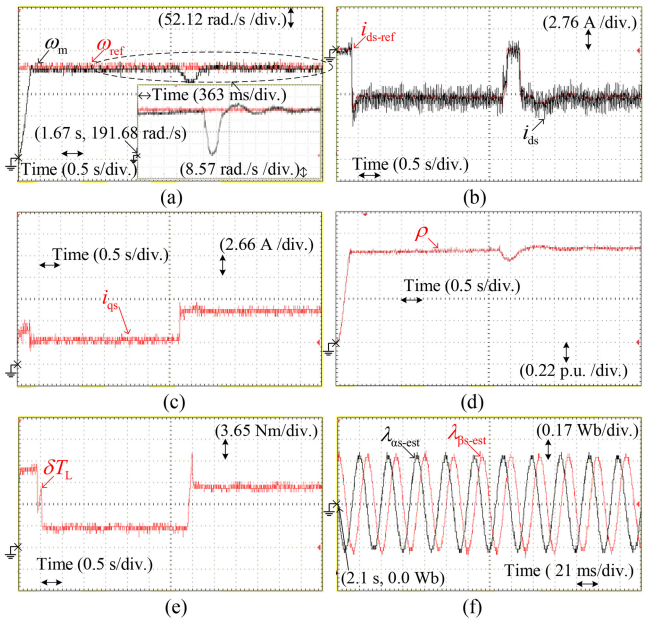

Fig. 18. Experimental results of the FOC strategy for the oscillation speed condition and torque disturbance, where (a) motor measured velocity and reference velocity (ω_m and ω_{ref}), (b) d-axis measured current (i_{ds}), and d-axis reference current, (c) q-axis measured current (i_{qs}), (d) voltage vector (ρ), (e) estimated torque (δT_L), and (f) estimated electromagnetic fluxes ($\lambda_{\alpha s\text{-est}}$, $\lambda_{\beta s\text{-est}}$).

The calculated torque and estimated axes fluxes for the proposed MPC, the classical MPC, and the FOC strategies are presented in Figs. 16(d) and (e), 17(e) and (f), and 18(e) and (f), respectively. Thus, the ADLPM of the proposed MPC can consider the variable operating torque to reduce speed drop, as well as the ripple of current and torque. Therefore, the peak of the

TABLE VII
TRADITIONAL STRATEGIES PERFORMANCE RELATIVE TO THE PROPOSED MPC FOR THE VELOCITY OSCILLATION STUDY

Items	Proposed MPC	Classical MPC	FOC
Settling time	0.42 s	1.5 times	4.4 times
Speed drop rate	12 rad/s	1.5 times	2.9 times
Steady-state error	0.5 rad/s	equal	5 rad/s
Mean i_{ds} (before torque disturbance)	−10.5 A	1.1 times	equal
Mean i_{ds} (after torque disturbance)	−11.9 A	1.1 times	equal
i_{ds} ripple	0.32 A	1.1 times	5 times
Mean i_{qs} (before torque disturbance)	0.23 A	1.3 times	1.2 times
Mean i_{qs} (after torque disturbance)	4 A	1.3 times	1.2 times
i_{qs} ripple	0.38 A	1.1 times	equal
Torque ripple	0.47 Nm	1.1 times	1.3 times

torque ripple is reduced under the proposed MPC by about 2.3% relative to the classical MPC and about 21.9% relative to the FOC. Meanwhile, the voltage vectors in Figs. 16(f), 17(d), and 18(d) indicate that the motor is in the flux-weakening region. Besides, the efficiency of the controlled PMSM is low due to it being unable to operate at the rated speed besides the rated torque. As a result, the motor efficiency is about 56.2%, 56%, and 55% for the proposed MPC, classic MPC, and FOC, respectively. Finally, Table VII summarizes the superiority of the performance of the proposed MPC compared to the classical MPC and FOC strategies for the velocity oscillation and load torque disturbance study.

VI. CONCLUSION

The MPC algorithms have sparked a lot of research, whereas flux-weakening operation in PMSM drives has not received much attention so far. Therefore, the main contributions in this article can be summarized as follows.

1) The proposed MPC strategy updates the internal time-invariant linear model at every prediction time around the operating conditions over different speed-field regions.
2) The online estimation of the induced torque and stator winding inductance has been proposed based on the TOGI observer.
3) The proposed cost function directly depicts the performance of the motor based on the velocity error and d-axis current error without dependence on the PI controller.
4) The proposed PCA calculates the modified reference velocity, d-axis demagnetization current, and maximum magnitude of the stator current. Thus, the rotor acceleration of the PMSM is controlled to obtain a stable speed and less current ripple.

Thus, the proposed MPC algorithm has been validated in comparison with the classical MPC and the FOC through case studies to include scenarios, such as velocity change, machine parameters variation, velocity fluctuation, and load torque disturbance. As a result, the obtained results have demonstrated the excellent dynamic capability of the proposed strategy. Meanwhile, the new method can take advantage of fast switching between speed regions, which can effectively reduce speed drop. Besides, it can reduce the current ripple, torque ripple, and transient period compared to the traditional strategies.

Finally, this article presents an improved adaptive discrete linear plant model that can be extended as future work to fast any real-time optimization technique of the MPC algorithm and enhance the prediction performance.

REFERENCES

[1] T. Geyer, *Model Predictive Control of High-Power Converters and Industrial Drives*. Hoboken, NJ, USA: Wiley, 2017.
[2] W. Xu, R. Islam, and M. Pucci, *Advanced Linear Machines and Drive Systems*. Berlin, Germany: Springer, 2019.
[3] J. Zou, W. Xu, X. Yu, Y. Liu, and C. Ye, "Multistep model predictive control with current and voltage constraints for linear induction machine based urban transportation," *IEEE Trans. Veh. Technol.*, vol. 66, no. 12, pp. 10817–10829, Dec. 2017.
[4] Y. Jiang, W. Xu, C. Mu, and Y. Liu, "Improved deadbeat predictive current control combined sliding mode strategy for PMSM drive system," *IEEE Trans. Veh. Technol.*, vol. 67, no. 1, pp. 251–263, Jan. 2018.
[5] J. Zou, W. Xu, J. Zhu, and Y. Liu, "Simplified model predictive thrust control based arbitrary two voltage vectors for linear induction machines in metro transportation," *IEEE Trans. Veh. Technol.*, vol. 69, no. 7, pp. 7092–7103, Jul. 2020.
[6] A. K. Junejo, W. Xu, C. Mu, M. M. Ismail, and Y. Liu, "Adaptive speed control of PMSM drive system based a new sliding-mode reaching law," *IEEE Trans. Power Electron.*, vol. 35, no. 11, pp. 12110–12121, Nov. 2020.
[7] Z. Li, P. Wang, H. Liu, Y. Hu, and H. Chen, "Coordinated longitudinal and lateral vehicle stability control based on the combined-slip tire model in the MPC framework," *Mech. Syst. Signal Process.*, vol. 161, Dec. 2021, Art. no. 107947.
[8] M. M. Ismail, W. Xu, Y. Liu, A. K. Junejo, and M. G. Hussien, "Improved controller optimization of flux-weakening strategy for salient permanent-magnet synchronous motor based on genetic algorithm," in *Proc. IEEE Energy Convers. Congr. Expo.*, 2021, pp. 4927–4932.
[9] M. M. Ismail et al., "Performance enhancement of salient permanent-magnet motors over wide speed range based on finite-set model predictive control," in *Proc. IEEE Int. Conf. Predictive Control Elect. Drives Power Electron.*, 2021, pp. 75–80.
[10] L. Samaranayake and S. Longo, "Degradation control for electric vehicle machines using nonlinear model predictive control," *IEEE Trans. Control Syst. Technol.*, vol. 26, no. 1, pp. 89–101, Jan. 2018.
[11] L. Chen, H. Xu, X. Sun, and Y. Cai, "Three-vector-Based model predictive torque control for a permanent magnet synchronous motor of EVs," *IEEE Trans. Transp. Electrific.*, vol. 7, no. 3, pp. 1454–1465, Sep. 2021.
[12] W. Xu, M. M. Ismail, Y. Liu, and M. R. Islam, "Parameter optimization of adaptive flux-weakening strategy for permanent-magnet synchronous motor drives based on particle swarm algorithm," *IEEE Trans. Power Electron.*, vol. 34, no. 12, pp. 12128–12140, Dec. 2019.
[13] M. M. Ismail, W. Xu, X. Wang, A. K. Junejo, Y. Liu, and M. Dong, "Analysis and optimization of torque ripple reduction strategy of surface-mounted permanent-magnet motors in flux-weakening region based on genetic algorithm," *IEEE Trans. Ind. Appl.*, vol. 57, no. 4, pp. 4091–4106, Jul./Aug. 2021.
[14] T. Englert, S. Grüner, and K. Graichen, "Model predictive torque control of permanent magnet synchronous machines," *IFAC-PapersOnLine*, vol. 50, no. 1, pp. 758–763, 2017.
[15] M. Preindl and S. Bolognani, "Model predictive direct torque control with finite control set for PMSM drive systems, part 2: Field weakening operation," *IEEE Trans. Ind. Inform.*, vol. 9, no. 2, pp. 648–657, May 2013.
[16] O. Arpacik and M. M. Ankarali, "An efficient implementation of online model predictive control with field weakening operation in surface mounted PMSM," *IEEE Access*, vol. 9, pp. 167605–167614, 2021.
[17] Y. Zhang and R. Qi, "High-Efficiency flux weakening drive for IPMSM based on model predictive control," *IEEE Trans. Transp. Electrific.*, p. 1, early access, Mar. 2022, doi: 10.1109/TTE.2022.3160454.
[18] Z. Zheng and D. Sun, "Model predictive flux control with cost function-based field weakening strategy for permanent magnet synchronous motor," *IEEE Trans. Power Electron.*, vol. 35, no. 2, pp. 2151–2159, Feb. 2020.
[19] Z. Zheng, D. Sun, M. Wang, and H. Nian, "A dual two-vector-based model predictive flux control with field-weakening operation for OW-PMSM drives," *IEEE Trans. Power Electron.*, vol. 36, no. 2, pp. 2191–2200, Feb. 2021.
[20] S. Fan, Y. Zhang, J. Jin, X. Wang, and C. Tong, "Deadbeat predictive current control of PMSM drives with an adaptive flux-weakening controller," *IET Power Electron.*, vol. 15, pp. 753–763, Feb. 2022.

[21] E. Fuentes, C. A. Silva, and R. M. Kennel, "MPC implementation of a quasi-time-optimal speed control for a PMSM drive, with inner Modulated-FS-MPC torque control," *IEEE Trans. Ind. Electron.*, vol. 63, no. 6, pp. 3897–3905, Jun. 2016.
[22] C. Ma, X. Yao, H. Li, and F. D. Belie, "Setting up reference variants to comply with current boundary settings in finite set model predictive PMSM control," *IEEE J. Emerg. Sel. Topics Power Electron.*, vol. 9, no. 5, pp. 5377–5389, Oct. 2021.
[23] X. Zhang and Z. Zhao, "Multi-stage series model predictive control for PMSM drives," *IEEE Trans. Veh. Technol.*, vol. 70, no. 7, pp. 6591–6600, Jul. 2021.
[24] Y. Zhang and R. Qi, "Flux-weakening drive for IPMSM based on model predictive control," *Energies*, vol. 15, Mar. 2022, Art. no. 2543.
[25] J. Liu, C. Gong, Z. Han, and H. Yu, "PMSM model predictive control in flux-weakening operation using an improved algorithm," *IEEE Trans. Ind. Electron.*, vol. 65, no. 12, pp. 9378–9387, Mar. 2018.
[26] Z. Mynar, L. Vesely, and P. Vaclavek, "PMSM model predictive control with field-weakening implementation," *IEEE Trans. Ind. Electron.*, vol. 63, no. 8, pp. 5156–5166, Apr. 2016.
[27] D. Bertsekas, *Nonlinear Programming*, 2nd ed. New York, NY, USA: Athena Scientific, 1999.
[28] A. Bemporad, "A quadratic programming algorithm based on nonnegative least squares with applications to embedded model predictive control," *IEEE Trans. Autom. Control*, vol. 61, no. 4, pp. 1111–1116, Apr. 2016.
[29] Y. Wang and S. Boyd, "Fast model predictive control using online optimization," *IEEE Trans. Control Syst. Technol.*, vol. 18, no. 2, pp. 267–278, Mar. 2010.
[30] Y. Jiang, W. Xu, C. Mu, J. Zhu, and R. Dian, "An improved third-order generalized integral flux observer for sensorless drive of PMSMs," *IEEE Trans. Ind. Electron.*, vol. 66, no. 12, pp. 9149–9160, Dec. 2019.
[31] Z. Q. Zhu, D. Liang, and K. Liu, "Online parameter estimation for permanent magnet synchronous machines: An overview," *IEEE Access*, vol. 9, pp. 59059–59084, 2021.
[32] M. Eull and M. Preindl, "An optimization-based reduced sensor virtual flux observer for PM synchronous machines," *IEEE Trans. Ind. Electron.*, vol. 68, no. 5, pp. 4320–4330, May 2021.
[33] A. Bemporad, M. Morafi, and N. Ricker, *Model Predictive Control Toolbox: User's Guide*. Natick, MA, USA: MathWorks. [Online]. Available: https://www.mathworks.com/help/pdf_doc/mpc/mpc_ug.pdf
[34] T. Takahama and D. Akasaka, "Model predictive control approach to design practical adaptive cruise control for traffic jam," *Int. J. Automot. Eng.*, vol. 9, pp. 99–104, 2018.
[35] H. Chuan, S. M. Fazeli, Z. Wu, and R. Burke, "Mitigating the torque ripple in electric traction using proportional integral resonant controller," *IEEE Trans. Veh. Technol.*, vol. 69, no. 10, pp. 10820–10831, Jul. 2020.

Moustafa Magdi Ismail received the B.E. and M.E. degrees in electrical engineering from the Minia University, Egypt, in 2011 and 2016, respectively, and the Ph.D. degree in 2021 with the school of Electrical and Electronics Engineering, State Key Laboratory of Advanced Electromagnetic Engineering of Huazhong University of Science and Technology, Wuhan, China. He has been awarded an Honorary International Graduate Certificate for his Ph.D. degree.

He is currently an Assistant Professor with Minia University. In 2021, he started teaching with El Minya Higher Institute of Engineering and Technology. He has published scientific papers in both international conferences and high-quality SCI journals. His current research interests include electric machinery, inverter systems, smart grids, modeling and control design of electric vehicles, predictive plant models, predictive control designs, and optimization algorithms.

Prof. Ismail is currently a reviewer for IEEE transactions journals such as IEEE TRANSACTIONS ON VEHICULAR TECHNOLOGY, IEEE TRANSACTIONS ON INDUSTRIAL ELECTRONICS, IEEE TRANSACTIONS ON TRANSPORTATION ELECTRIFICATION, IEEE Transactions on Power Electronics, IEEE TRANSACTIONS ON ENERGY CONVERSION, and IEEE TRANSACTIONS ON INDUSTRY APPLICATIONS, IEEE JOURNAL OF EMERGING AND SELECTED TOPICS IN INDUSTRIAL ELECTRONICS, and IEEE ACCESS. He has been selected as one of the Top Reviewers of IEEE TRANSACTIONS ON VEHICULAR TECHNOLOGY in 2020.

Wei Xu (Senior Member, IEEE) received the double B.E. and M.E. degrees in electrical engineering from Tianjin University, Tianjin, China, in 2002 and 2005, respectively, and the Ph.D. degree in electrical engineering from the Institute of Electrical Engineering, Chinese Academy of Sciences, Beijing, China, in 2008.

From 2008 to 2012, he was a Postdoctoral Fellow with the University of Technology Sydney, the Vice-Chancellor Research Fellow with the Royal Melbourne Institute of Technology, and a Japan Science Promotion Society Invitation Fellow with Meiji University. Since 2013, he has been a Full Professor with the State Key Laboratory of Advanced Electromagnetic Engineering, Huazhong University of Science and Technology, Wuhan, China. His research topics mainly cover design and control of linear/rotary machines.

Prof. Xu is Fellow of the Institute of Engineering and Technology. He was the General Chair for 2021 International Symposium on Linear Drives for Industry Applications (LDIA 2021), Wuhan, China, and 2023 IEEE International Conference on Predictive Control of Electrical Drives and Power Electronics (PRECEDE 2023) , Wuhan, China. He was/is an Editor or Associate Editor for more than ten internationally leading journals, such as IEEE TRANSACTIONS ON INDUSTRIAL ELECTRONICS, IEEE TRANSACTIONS ON VEHICULAR TECHNOLOGY, IEEE TRANSACTIONS ON ENERGY CONVERSION, and IEEE TRANSACTIONS ON INDUSTRY APPLICATIONS.

Jian Ge was born in Heilongjiang, China, in 1994. He received the B.E., M.E., and Ph.D. degrees in electrical engineering from Huazhong University of Science and Technology, Wuhan, China, in 2016, 2019, and 2022, respectively.

He is currently a Postdoctoral Researcher in electrical engineering with Huazhong University of Science and Technology. His research interests include induction machines, linear machines, and brushless doubly fed machines.

Yirong Tang (Student Member, IEEE) received the B.E. degree in electrical engineering in 2020 from Huazhong University of Science and Technology, Wuhan, China, where he is currently working toward the Ph.D. degree with the State Key Laboratory of Advanced Electromagnetic Engineering and Technology.

His research interests include advanced control methods for permanent magnet synchronous machines, linear induction machines, and drives.

Abdul Khalique Junejo (Member, IEEE) was born in Larkana, Sindh province, Pakistan, in 1989. He received the B.Sc. and M.Sc. degrees in electrical engineering from Quaid-e-Awam UEST Nawabshah, Sindh Pakistan in 2011 and 2015, respectively, and the Ph.D. degree from the School of Electrical and Electronics Engineering, State Key Laboratory of Advanced Electromagnetic Engineering, Huazhong University of Science and Technology, Wuhan, China.

He is currently an Assistant Professor with Quaid-e-Awam UEST. He authored or coauthored 15 SCI journal papers including 8 IEEE papers, such as IEEE TRANSACTIONS ON VEHICULAR TECHNOLOGY, IEEE TRANSACTIONS ON POWER ELECTRONICS, IEEE TRANSACTIONS ON ENERGY CONVERSION, IEEE TRANSACTIONS ON INDUSTRY APPLICATIONS, and IEEE Access, 1 Emerging Sources Citation Index, and 15 national and international journals. Furthermore, he also attended and presented at international conferences on machines including International Conference on Electrical Machines and Systems, LIDA, and IEEE Energy Conversion Congress and Exposition. His research interests include sliding mode control, direct torque control, model predictive control, and sensorless control methods for permanent magnet synchronous machines, induction machines, linear IM and drives, and renewable energies.

Prof. Junejo was a Reviewer for IEEE journals such as IEEE TRANSACTIONS ON INDUSTRIAL ELECTRONICS, IEEE TRANSACTIONS ON POWER ELECTRONICS, IEEE TRANSACTIONS ON TRANSPORTATION ELECTRIFICATION, IEEE TRANSACTIONS ON INDUSTRY APPLICATION SOCIETY, Emerald Group Publishing Ltd., *Assembly Automation*, and IEEE JOURNAL OF EMERGING AND SELECTED TOPICS IN INDUSTRIAL ELECTRONICS.

Mohamed G. Hussien (Graduate Student Member, IEEE) was born in Zefta, Gharbeya, Egypt, in 1988. He received the B.Sc. and M.Sc. degrees in electrical engineering from the Department of Electrical Power and Machines Engineering, Faculty of Engineering, Tanta University, Tanta, Egypt, in 2011 and 2016, respectively, and the Ph.D. degree from the School of Electrical and Electronic Engineering, Huazhong University of Science and Technology, Wuhan, China, in 2020.

He is currently an Assistant Professor with the Department of Electrical Power and Machines Engineering, Faculty of Engineering, Tanta University. He has authored or coauthored scientific papers in both international conferences and high-quality SCI journals. His research interests include electrical machine analysis, electrical drives, electric vehicles, sensorless control, doubly fed machines, power electronics, and renewable energy systems.

Prof. Hussien is a member of the IEEE-IES Electric Machines Technical Committee and the IEEE-IES Technical Committee on Renewable Energy Systems. He is currently an Associate Editor for the *IET Renewable Power Generation* journal. He is also currently an Editorial Board Member for the *Distributed Generation & Alternative Energy Journal* and a Reviewer for several IEEE conferences and journals, including IEEE ACCESS, IEEE TRANSACTIONS ON INDUSTRIAL ELECTRONICS, and IEEE TRANSACTIONS ON POWER ELECTRONICS. He was a Guest Editor for *Energies* journal. His paper was selected as one of the best papers published in the period (2019–2020) in the IEEE TRANSACTIONS ON ENERGY CONVERSION in the "Power generation systems and grid interfaces" area. He was the recipient of the Best Paper Award from the IEEE IAS GUCON 2021 conference.